Original Article

Monitoring of hole surface integrity in drilling of bi-directional woven carbon fiber reinforced plastic composites

**Tarakeswar Barik[1], Kamal Pal[1] , Smruti Parimita[1],
Priyabrata Sahoo[2] and Karali Patra[2]**

Abstract

Fiber-reinforced plastic is one of the top priorities lightweight materials with excellent mechanical properties for the aerospace industries in recent years. However, it is difficult to machine despite having unique properties due to its non-homogeneous and abrasive nature in alternate fiber and matrix layers. Thus, it is found to be a challenging task to drill hole on such hard-to-machine materials, which is highly essential for the development of most of the engineering structural components. The present work addresses various drilling-induced defects such as delamination, circularity error, and roughness variations in the hole surface during drilling of quasi-isotropic cross-fiber oriented bi-directional woven-type carbon fiber reinforced plastic laminate using a full factorial design of experiments for different drill geometry. The response surface methodology was considered for the regression model development, which was found to be highly significant. The machining forces with associated torque have also been acquired during drilling, which was divided and further analyzed in time domain to correlate with drilling flaws. The drilling-induced delamination was found to be higher at a high feed rate using a higher drill point angle due to substantial thrust force generation at the initial stages in the drilling cycle. However, the internal surface finish with associated circularity error was reduced for higher spindle speed with less feed rate using a low drill point angle because of low torque fluctuation at the final drilling phases. The axial thrust force was found to be a prime indicator of drilled hole surface delamination, whereas drilling torque precisely indicated internal surface roughness as well as circularity error. The global root mean square, along with a local peak of thrust and torque, both were highly essential to completely characterize the drilled hole quality.

Keywords

CFRP, thrust force, torque, quasi-isotropic, delamination, circularity error

Date received: 4 October 2019; accepted: 3 January 2020

Introduction

The engineering materials have to fulfill the design necessities with ease in manufacturability as well as economical to the end-users. The need for superior materials having a high strength to weight ratio like fiber-reinforced plastics during the past decades is found to be significantly increased in aerospace, automobile, marine, and sports goods manufacturing industries.[1–5] These advanced materials can also sustain high impact loads at altered time intervals with a high degree of corrosive resistance because of the specific macroscopic combinations of fibers (reinforcement phase) and polymer matrix (matrix phases) in this fiber-reinforced laminates.[1,3,6–8] The reinforcements are strong, stiff, and brittle, which is mixed with the soft and pliable matrixes. Thus, these advanced materials are also the primary choice for structural engineers in aerospace, marine, and defense sectors.[2,3]

The fibers provide the strength to the composite laminate, and the matrix binds the fibers together while transferring the load to the adjacent fibers as well as acts as a safeguard from the outer environment. As the reinforcing materials are fibers, these laminates/materials are called as fibrous composites or fiber-reinforced plastics (FRPs).[9] These FRPs

[1]Department of Production Engineering, Veer Surendra Sai University of Technology, Odisha, India
[2]Department of Mechanical Engineering, Indian Institute of Technology Patna, Bihar, India

Corresponding author:
Kamal Pal, Department of Production Engineering, Veer Surendra Sai University of Technology, Burla, Sambalpur, Odisha 768018, India.
Email: kpal5676@gmail.com

popularly used a continuous or discrete form of fibers, out of which the continuous fibers are beneficial over the later one.[7,10] The continuous fibers are a unidirectional or bi-directional category. The bi-directional type is formed by placing the thin uni-directional fibers called prepreg in a woven system. The uni-directional and bi-directional groups both have superior properties. The uni-directional prepregs indicate high stiffness and strength along the fiber direction rather than in the perpendicular, named as anisotropic material.[7,10] However, the bi-directional prepregs strengthened in both the directions, called quasi-isotropic materials, make it preferable in most of the engineering applications. On the other hand, the laying up and orientation of the reinforcing fibers is strongly correlated with the fabrication end-properties as the fibers are subjected to compression, bending, and cutting action during drilling, which in turn found to be a challenging task to the manufacturers.[11] Thus, the fiber is sheered, and rough surfaces have resulted in machining when fibers are lied inclined at 45° angle with cutting direction, whereas the fibers undergo flexion if this orientation angle is perpendicular (90°) resulted in smooth surface.[7,10,12] However, the fibers are subjected to undergo bending and shear, resulting in tearing of fiber when the fibers have been negatively inclined (−45° angle) to the cutting direction.[10] Finally, these prepregs have been stacked together by applying a polymer matrix of a thermoplastic or thermosetting set to form the composite laminates.[10] The thermoplastic polymer matrix has better mechanical properties at high temperature with a high degree of ease during manufacturing.

The fiber-reinforced composites may be categorized as per the reinforcing fibers like glass fiber-reinforced plastics (GFRPs),[13] carbon fiber-reinforced plastics (CFRPs),[7,12] and combination of both fiber and metal composite namely fiber metal composite laminate (FML).[2,3,14] These materials can reduce the total weight up to 50% in Boeing and airbus like the one airliner utilizes that in accommodating extra baggage.[1,3,5] The GFRPs are found to be used in making passenger compartments, room doors, and landing gear doors.[1,10] The CFRPs are applied to manufacture wing panels, j-nose, and stabilizers, whereas CFRPs with metal stack form of aluminum and titanium are used in making fuselages, wings, keel beam, and tails.[2,15,16] However, a secondary process like milling, drilling, and trimming is often highly essential for the final assembly.[17] Thus, the final structural components are found to be comprised of riveted joints for which drilling operation is generally recommended as a cost-effective and time-efficient strategy.[18] The mechanical fastening, such as riveting, bolting of the different subassemblies of the complete structural body used in several engineering applications, is highly essential. It necessitates secondary machining processes like drilling for making holes in the structural elements. However, drilling holes through the composite laminates is somewhat different from metal as the drill encounters plastic (matrix phase) and fiber (reinforcement phase) alternatively, characterized by the drastic difference in their mechanical and thermal properties. Thus, it is relatively difficult for the machining of these hybrid materials. Moreover, the joining efficiency of the bolted and riveted joints primarily depends on the quality of the drilled holes.[19–21] Therefore, a drilled hole should be uniform without any surface defect to achieve adequate joint strength with high degree precision for interchangeability.

The CFRP composites are found to be ambiguous to machine irrespective of their superior mechanical properties. Thus, there is a growth in the research works that have been noticed in the selection of fiber orientation in the fabrication of fibrous laminates as well as their machinability aspects in recent years. There are successions of shear fracture found to have occurred in the fibers and matrix through which the load distribution somewhat uneven during the drilling of CFRPs. On the other hand, highly abrasiveness, material discontinuity, inhomogeneity, and anisotropic nature of these materials also deteriorate the machinability of such materials rather than metals. Various surface damages and irregularities like fiber cracking, delamination, fiber burnout, fiber pullout, spalling, matrix cracking, debonding, chipping, circularity error, and high roughness factor are significant during drilling. Thus, the strength of the laminate against fatigue, impact loading, and demeaning the performance substantially reduces. The delamination is generally considered the top and exit surface defect of a drilled hole, which supports the nut or rivet during mechanical fastening processes. It is an inter-ply failure phenomenon due to which almost 60% of the engineering products have been turned into scarps in the final assembly lining each year.[22] The laminate fibers are subjected to compression as well as bending during drilling, which is responsible for the lifting or peeling of fibers resulted in delamination. On the other hand, the inherent heterogeneity and high abrasiveness in carbon fibers drill bits wear out very rapidly, which leads to severe disfigurement of the drilled hole.[23]

In drilling operations, the cutting edges are responsible for cutting the materials, whereas the flutes are responsible for guiding the cutaway materials to come out. Since the material is not properly cut away from the adjacent layer due to the fibers' bonding, the peeling action from the concerned layers is found to have occurred. The cutting forces have proceeded toward the peripheral direction, which enhances the peeling of fibers, resulted in peel-up delamination or delamination at entry-level. In the last phases in the drilling cycle, the uncut thin layer of prepregs present beneath the drill becomes very weak and subject to deformation when the drill penetrates the drilled hole. The axial thrust force reaches its lowest level during this

stage, which often exceeds the inter-laminar bonding strength; thus, materials present beneath the drill push out of the hole in the form of push-out delamination.[18] However, this exit stage delamination occurring chances are less in comparison to the pull-up delamination at the entrance as the thrust force reaches its lowest value.

The delamination damage is considered as the central failure regardless of the fiber type in FRPs, which may be characterized by the separation of physical layers of materials in a hole. Therefore, it is generally considered a vital means of failure as it may disturb the tensile properties and durability as well as a reduction in the bearing strength and structural integrity of the composite laminate, which in turn influences the performance issues. Delamination cannot be eradicated, like welded plate distortions, but can be reduced with proper adjustments of machining parameters like feed rate, spindle speed, drill geometry, etc. The delamination is found to be increased with a higher feed rate due to stronger thrust force using different drill bits in FRPs.[1,3,13,22–25] However, it can be improved to some extent by increasing the spindle speed in the drilling of bi-directional composite laminates.[26–29] This surface damage-related defect is also found to be observed in high-speed drilling of thin woven-ply carbon fiber composite laminates due to quick tool wear, which in turn increases the thrust force.[19,26,30,31] Thus, the drill-induced defects were significantly increased at higher feed rate.[28] The drill point angle is also profoundly influenced the delamination with an increase in the case of the WC (tungsten carbide) twist drill due to the same reason. The thrust force should be lower than a specific range called a critical thrust force to achieve a delamination free hole. Besides that, if the orthogonal rake angle of the drill tool at each point on the primary cutting edge is increased using a high helix angle, it may also reduce the thrust force. The drilling-induced thrust force increases with an increase in drill web thickness, which again varies with the chisel edge length.[5] The higher thrust force development leads to various types of wear and hence shortens the tool life. However, there is a small increase in thrust force for the early stages of a drill, which is later predominantly increased at later stages of the drill service life.[32] The effect of tool materials on the quality of holes also cannot be neglected. Carbide drill has better performance than HSS drill concerning delamination in drilling CFRPs.[3,8] However, the excessive heat generation during the drilling of CFRPs is another aspect of the assessment of machinability.[33] The major contribution to the overall heat generation is the heat developed along with the work-tool flank interface, which is proportional to primary drilling parameters, i.e. cutting speed and feed rate.

The machinability of CFRPs depends upon various drill's geometry factors like point angle, primary and secondary cutting edges, size of chisel edge, and drill material. Although the initial axial thrust force by the drill on the work is higher, it is significantly reduced at a higher speed. Thus, the fibrous material softens for which drill bit smoothly extrudes the material. Moreover, the tool wear or edge chipping is predominantly higher using drills without any chisel edge like brad and spur or dagger having straight flutes due to sharp corners that sustain the bulk of the cutting load.[34] Thus, the tool stability deteriorates with time without the presence of core during drilling resulted in poor drilled hole quality along with inadequate chip disposal resulted in more power requirement, particularly in mass production. On the other hand, the twist drill flutes comprised of sharp guide champers was found to be beneficial in removing the uncut fibers and guide the tool in the hard to machine material like CFRPs. Besides, the secondary cutting edge is also helpful in removing the cut chip stuck in the material which has not found using "Dagger drill bit."[17,28] The circularity, roundness, and concentricity of the drilled hole are also considered with delamination for the acceptability of the hole for which a conventional twist drill may be recommended.

The preceding summary on a literature survey on the machinability of CFRP composite indicated that there were several works on parametric influence on surface delamination and internal surface roughness as performance parameters in drilling. However, the interaction effect of drill spindle speed and feed rate using different tool geometry on the surface delamination factor was not investigated in detail. Moreover, the hole surface integrity characteristics such as circularity error as well as roughness not properly presented using profile graphs. Thus, the present work addresses the interaction effect of process variables on these hole quality characteristics with different drill geometry on fabricated bi-directional woven in detail. On the other hand, though there were some works on process monitoring of CFRP drilling, there was hardly any work on time-domain statistical feature analysis of the thrust as well as torque phasewise in the drilling cycle. The sensitivity analysis has also been considered to search the significant statistical feature for the process monitoring, which was further extended to response surface modeling capability for the first time. The objective was to compare the prediction capability of drilled hole quality using different significant statistical parameters of thrust and torque in the developed models. Finally, the prediction error has also been analyzed globally, considering all the drilling experiments as well as individually to conclude the same precisely.

Experimental procedure

In the present work, the drilling experiments have been carried out on fabricated (manual hand layup method) quasi-isotropic CFRP composite laminates. This quasi-isotropic carbon fiber laminates

characterized by 10 mm thickness contained 16 layers of 0.5 mm thick carbon fiber prepreg plies stack together by epoxy resin (type-Araldite LY-556) mixed with hardener (type-Aliphatic amine HY-951). The stacking sequence of the woven-type bidirectional laminate was positioned $[0/-45/90/45]_{2s}$ during fabrication, so that it can sustain high load without much variation in the mechanical behavior along the loading direction.[34] The reinforcing carbon fibers used for fabrication have high tensile strength (6000 MPa). The piles of the prepregs have been kept inside a mild steel mold in which a uniform pressure was maintained during the curing of the laminates. The dimensional specification with mechanical properties of the carbon fiber laminate is

Table 1. Ingredients details for the fabrication of CFRP laminate.

Descriptions	Specifications
Fiber thickness	0.465 mm
Fiber tensile strength	6000 MPa
Matrix used	Epoxy-Araldite LY-556
Hardener used	Aliphatic amine HY-951
Work made-up process	Hand layup technique
Work dimension	200 mm × 200 mm × 10 mm
Work tensile strength	3000 N/mm^2
Job size for drilling	200 mm × 100 mm × 10 mm

Table 2. Geometrical specification of the drills used.

Drill geometry parameters	Drill 1 1	Drill 2	Drill 3
Diameter (mm)	10	10	10
Point angle (°)	110	118	128
Web thickness (mm)	0.121	0.140	0.160
Helix angle (°)	28.5	30	32
Clearance angle (°)	8.35	8.60	8.67

indicated in Table 1. However, the work sample to be drilled has been prepared with 200 mm × 100 mm × 10 mm dimensions using an electric gauge cutter.

In this work, three carbide twist drills having different point angles were considered for the drilling experiments. The detailed geometrical specification is shown in Table 2. The pre-wear on the drill tool due to several usages does a significant effect on the hole quality, such as the delamination factor influenced by feed rate and drill spindle speed due to subsequent variation of the thrust force and torque development during drilling. However, in the present work, a new tool has been taken for each drilling experiment (i.e. each parametric condition), so the tool wear effect was eradicated.

A CNC milling center (MTAB) with high power capacity (5 kW) was used for the drilling experiments. The experimental setup is shown in Figure 1. The limiting speed of this single-spindle vertical machining center is 5000 r/min with vertical feed capacity up to 3000 mm/min. The sampling rate of acquiring thrust force and torque signals was kept constant at 1 kHz throughout the drilling experiments in this work. However, in this experimental investigation, the data acquisition system has several highly sensitive peripherals hardware with inbuilt software for acquiring the force/torque signals. The piezoelectric-type dynamometer was fitted with the work which was mounted on the machine bed. The piezoelectric dynamometer (type KISTLER 9257b) and a KISTLER amplifier (model 5070) along with a data acquisition system have been used for the force/torque signals acquiring during drilling.[35] The data acquisition system comprised of data acquisition card integrated with DYNOWARE software (type 2825D-02) of the latest version (2.5.1.2) for accurate data capturing and further analysis. A dedicated fixture has been designed and developed to properly hold the laminated fibrous sample during drilling. In the present experimental work, the force with corresponding torque signals has been acquired at a sampling rate
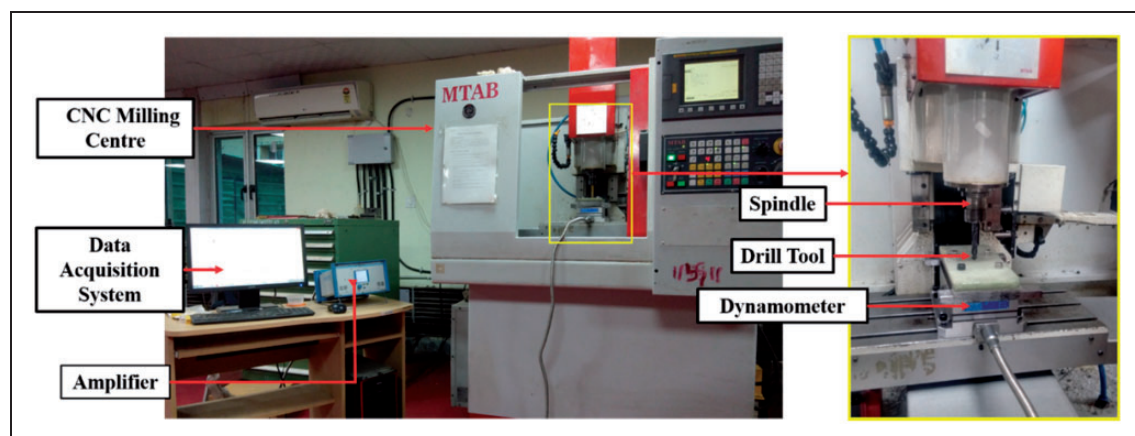

Figure 1. Experimental setup with work clamping arrangement on a dynamometer.

of 1000 Hz. The highest machining feed rate (at 3200 r/min spindle speed with feed rate 0.075 mm/rev) was 4 mm/s. Therefore, the total 1000 data have been acquired per one second during this high-speed drilling, i.e. distance between two consecutive addressable points along the working thickness was 0.004 mm, which is significantly accurate to characterize the dynamic nature of the process in terms of force and torque signals. Thus, for one revolution of the tool, the signals were acquired around $18.75 \approx 19$ data points per drill revolution (at 3200 r/min) to accurately analyze the pattern of the force/torque variation along the hole circumferential distance, which is sufficient enough for the same reason around the drilled hole surface development.

The selection of the available range of drilling parameters using the WC twist drill has been adjusted as per the previous literature reviewed.[3,34] However, a large number of trail experiments have been carried out with different combinations of speed and feed rates using three drill point angles for acceptable delamination, with good surface finish and less roundness error through which suitable, feasible cutting parameter range considering each drill point angle has been selected. The key objective was to investigate the influence of alteration in speed, feed, and point angle on the stated response outputs. Thus, a combination of slow (1225 r/min), moderated (2250 r/min), and relatively high speed (3200 r/min) was chosen. Similarly, three low feed rates of 0.025, 0.050, and 0.075 mm/rev were selected. Most importantly, a wide range of point angle ranges from 110° to 128° were chosen to understand the pattern of dynamic variation in thrust force and torque during drilling along with its adverse effect on the hole quality.[1,13,35]

These two primary process variables, namely spindle revolutions per minute and feed rate with three levels of each, have been considered for three different drill point angles (Table 3). The drilling experiments have been designed using a full factorial design of experiments using Minitab17 software, i.e. a total of 27 drilling experiments were carried out in this work. Some experiments (Expt. 14.) have been repeated two to three times to check the repeatability of the drilling machine.

Measurement of statistical features of sensors' signals

The axial force and torque signals have been acquired during the drilling experiments in real time which were further analyzed in time domain considering statistical mean, standard deviation, and root mean square (rms) using Microsoft Excel and Matlab software. The primary objective was to investigate their correlation with hole quality features to further monitor the process.

The average of some grouped sampled data of the respective signal defined as the sum of all the numbers in a group divided by the total number of samples present in that group. It may be expressed as

$$\mu = \frac{\sum_i^y}{N} \tag{1}$$

where y_i is the observation data set, μ is the mean of the observation data set, and N is the size of the observation data set.

The standard deviation (σ) is a measure of dispersion in statistics. It provides an inkling of how the individual data in a data set is detached from the mean. It is described as the square root of the mean of the squares of the deviations of all the values of a series derived from the arithmetic mean, also known as the rms deviation. It may be expressed as

$$\sigma = \sqrt{\frac{1}{N} \sum_{i=1}^{N} (y_i - \mu)^2} \tag{2}$$

where y_i the observation data set, μ is the mean of the observation data set, and N is the size of the observation data set.

The rms is generally recognized as the quadratic mean, which is used in statistics and mathematics. This formulation provides the total sum of the square root of each data in an observation. It is normally denoted by X_{rms}. It can be expressed as

$$X_{\text{rms}} = \sqrt{\frac{y_1^2 + y_2^2 + y_3^2 \ldots y_N^2}{N}} \tag{3}$$

where y_1, y_2 and y_3 are observations and N is the total number of observations.

The local peak value (p) is generally the maximum value of all the numbers in a group. It can be expressed as

$$p = \max(y_1, \ y_2, \ y_3 \ldots y_n) \tag{4}$$

Measurement of drilled hole characteristics

The delamination factor may be expressed as one-dimensional or two-dimensional factor in the measurement of a drilled hole. The one-dimensional delamination factor (F_d) is generally expressed as the ratio of the maximum diameter (D_{max}) to the nominal

Table 3. Drilling parameters with their levels.

Factors	Levels		
Speed (N) (r/min)	1225	2250	3200
Feed rate (f) (mm/rev)	0.025	0.05	0.075
Point angle (Ø) (°)	110	118	128

diameter ($D_{\min}$) of the delaminated drilled hole macrograph (equation (5)) which is indicated Figure 2.[24]

$$\text{Delamination factor,} \quad F_d = \frac{D_{\max}}{D_{\min}} \qquad (5)$$

The above expression holds good if the entry and exit level delamination is considered, as it is only focused on the upper few layers of the laminate in pull-up delamination at entry and bottom few layers in case of push-up delamination. However, if the delamination of the entire hole has to be considered, the variation from layer to layer has to be followed, which may be represented by using a two-dimensional delamination factor (D_f) as per equation (6)[14,36]

$$D_f = \left(\frac{A_{Del} - A_{Nom}}{A_{Nom}} \right)\% \qquad (6)$$

where A_{Del} is the delamination area and A_{nom} is the nominal area.

The drilling-induced delamination is a surface defect of the drilled hole developed during the entry and exit of the drill bit in drilling through the laminate, i.e. top and bottom layer known as pull-up and push-down delamination, respectively. However, it is not so significantly caused by fiber damage due to more stability just after insertion the drill point edges evidenced by uniform thrust force (stages III–V). Therefore, the one-dimensional delamination factor was considered in the present delamination analysis though there are higher dimensional measurement approaches for accurate quantification of delamination damage throughout the depth of drilled hole.[17] However, the circularity error (also called hole roundness error) has been measured throughout the drilled hole thickness using coordinate measuring machine (CMM), which is also a major indicator of interlaminar delamination factor throughout the depth of the hole. The surface roughness has also been measured in the same procedure using digital roughness tester along with this surface waviness study (i.e. circularity profile error) to characterize the surface integrity in a better way.

In the present work, the macrographs of the delaminated drilled hole were used in detailed delamination

Figure 2. Measurement of drilled surface delamination.

measurements using IMAGE J software on optical micrographs. This measurement process comprised of two major steps.[24] In this method, initially, the red, green, and blue images have converted to hue, saturation value (HSV) format, characterized by three respective levels. Out of these three levels, the second one, i.e. the saturation level, is generally utilized for diametric analysis in which a mask has been applied to convert it into BW image. Thus, it can adequately identify the drilled hole circumference. This BW image has been further smoothened for the exclusion of the uncut fibers. Then, the maximum diameter of the delaminated area, i.e. the white region between the two black boundaries has to be identified and measured. Subsequently, the minimum diameter of the nominal area with the shortest black boundary is identified, and this area has also been calculated. Then, the delamination factor (F_d) may be obtained by using the values of D_{max} and D_{min} in equation (5).

The SPECTRA ACCURA CMM with a ruby probe of 2 mm diameter has been used for the circularity error measurement of the drilled hole. The probe has been moved over the internal wall at different depth of the hole during each measurement. Thus, these measurements have been carried out on 10 different depths along with the hole depth from top to bottom at 1 mm intervals. The scanning rate of the measuring probe was set at 1 mm/s while revolving around the inner surface of the hole. Thus, the circularity error value was obtained from CMM. The internal surface roughness of the drilled hole has been measured using Talysurf roughness tester fitted with a diamond probe of 2.78 μm. The tester used has a cut-off length of 0.8 mm, cutting depth of 30 μm, and bandwidth of 5 μm. However, the sample length was set at 3.5 mm for the roughness measurement. The roughness tester has been moved over the internal surface repeatedly four times, two from each side of the hole, and the average value has been calculated for further analysis. The significant sensor-based features with corresponding process parametric settings have been further used for the prediction of these drilled hole quality characteristics. The procedural steps of the present work for the process monitoring have been summarized in Figure 3.

Result and discussion

The parametric influence on drilled hole surface quality features such as delamination, surface roughness, and circularity error has been studied in detail. The variation of sensor-based significant statistical parameters with drill spindle revolutions per minute and feed rate has also been investigated in the time domain using different drill point angles. The peak and rms value of the axial thrust force with corresponding torque were considered in this work. However, the profile of thrust force and torque signals of most of the drilling experiments was found to be almost the same. Thus, a typical
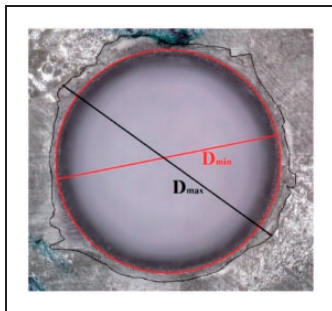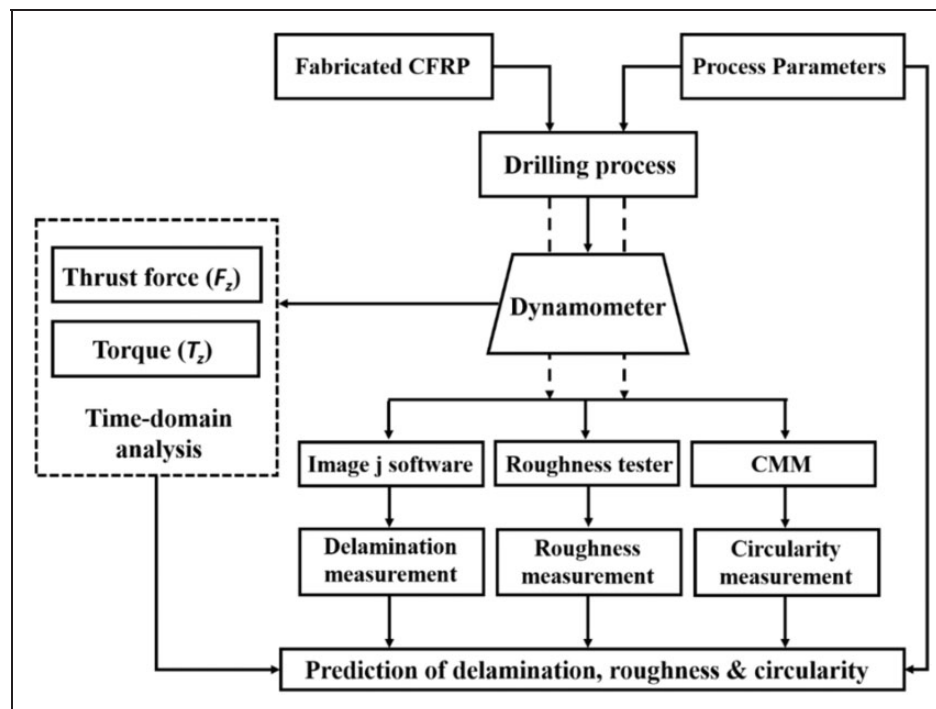
Figure 3. Schematic illustration of the procedural work plan for process monitoring.

thrust force with associated torque signals was studied in the time domain during different phases of drilling operation for CFRP composite using a twist drill is shown in Figure 4 (Expt. 1). Seven distinct phases (I–VII) starting from drill contact to departure through the work laminate have been identified, where significant variation was noticed in force or torque or both signals, as indicated by vertical dotted line.[4,18,27] The rms value of thrust force and torque of the seven distinct phases in Expt. 1 has also been indicated in Figure 5. These different drilling phases have been discussed in the following sections.

Phase I: Contact of the drill bit to CFRP laminate

In this phase, the drill bit touches the CFRP layer and approaches into the laminate. The chisel edge of the drill bit tears the CFRP laminate in this phase. Thus, the thrust force, as well as torque, was found to be sharply increased as the chisel edge penetrated the work. It was mainly due to the extrusion or pushing of material by the chisel edge. This stage is highly crucial as entry delamination occurs with drill bit off-setting, which influenced the roundness of the hole. This phase duration was about 3–5 s. The rms value of force and torque was found to be 12.7 N and 0.3 Nm, respectively, as shown in Figure 5.

Phase II: Entrance of the drill lips into CFRP laminate

The material removal starts at the beginning of this phase. In this phase, the cutting lips encounter work

material, and thus, the thrust force, as well as torque, was found to be increased smoothly (i.e. not so sharply). This phase also continued about 5–7 s as shown. The axial thrust force was found to relatively more fluctuate than torque in this phase. It was primarily due to the air gap present between piles in the respective laminate during fabrication.[36] The thrust force variation was more predominant with a thicker entrapped air gap in between prepregs. Thus, this air gap variation did not highly influence the torque required during drilling. In this phase, drilling-induced problems such as surface delamination generally found to be observed due to non-uniform and higher axial thrust force. The rms force, as well as rms torque, was increased significantly (72.4 and 73.3%, respectively) as indicated in Figure 5.

Phase III: Initiation of stable drilling

In this stage, the drill lips are completely inserted into the composite laminate without any chance of drill bit offsetting from the drilling center. It may be due to more area of contact of the drill bit with the laminate as the whole wedge surface is engaged in this short duration phase (2–4 s). Thus, the drilling process is relatively stable for which there was a slight drop in thrust force as well as torque constraint. However, the torque reduction was found to be more predominant, as shown in Figure 4. The rms value of both axial thrust and torque was slightly increased concerning phase II as shown.
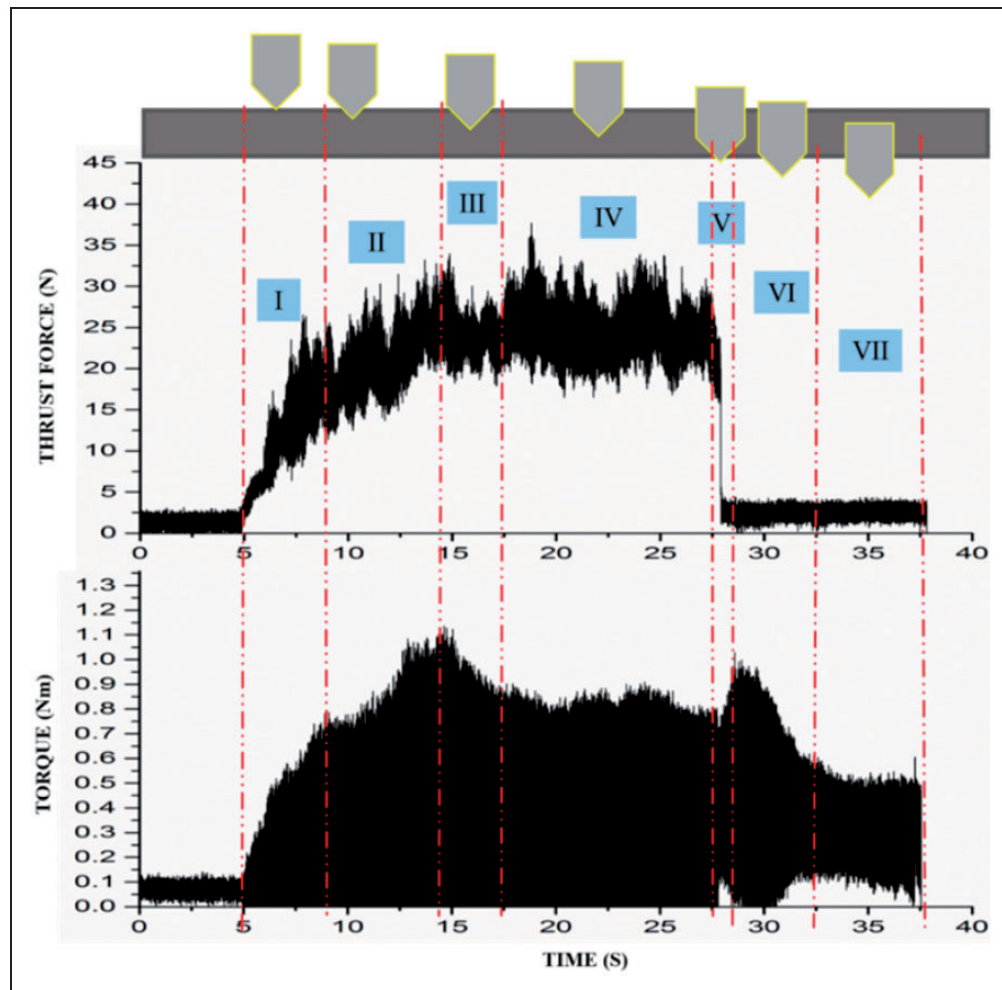
Figure 4. Variation of thrust force and torque in different stages of the drilling cycle.
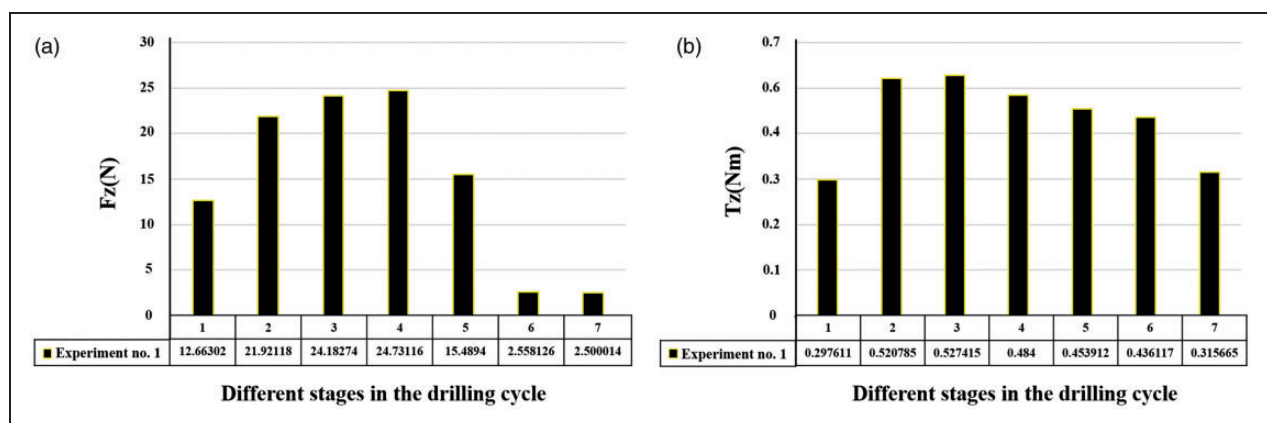
Figure 5. Variation of (a) rms force and (b) rms torque in different phases during drilling (Expt. 1).

Phase IV: Stable drilling

This is the primary phase of the drilling cycle in which machining chips are removed through the drill bit helix grooves. It is the most prolonged phase of drilling as shown (9–11 s). Thus, the thrust force, as well as the torque, was found to be constant with slight fluctuation due to air gap induced composite laminate as shown. The axial thrust variation was more significant than torque indicated this air gap defect. However, the material removal rate was uniform, evidenced by uniform torque generation. This phase continued until the chisel edge reached the bottom last pile of the laminate. The peak, as well as root, mean square value of the axial thrust force was found to be the highest because of machining chips gathering

through the drill flutes, i.e. fully loaded drill state in this phase. However, the rms thrust force and torque were found to be the same as in phase III.

Phase V: Final phase of through-hole generation

In this phase, the through-hole is just completed when the drill reaches the last prepregs of the laminate. The chisel edge is out of contact with the work because of which surrounding materials around the pilot hole (formed by chisel edge) attempt to grip the drill wedge circumference in this phase. Thus, the thrust force was found to be significantly dropped down instantaneously (within 1–3 s) to the ground state with a sharp increase in torque as shown. However, a sudden fall of drilling torque has been noticed just before this sharp increase, possibly due to the spring back effect of the uncut fibers of the laminate around the pilot hole. However, the rms value of torque was slightly reduced (6.3%), whereas rms axial thrust reduction was found to be significant (37.3%) concerning the previous phase.

Phase VI: Completion of through-hole development

In this phase, the cutting lips of the drill are entirely out of contact with the work indicated end of chip generation. Therefore, the machining torque sharply reduced to the ground state, whereas the axial force was found to be the same in this phase as expected. However, the torque at the ground state just after through-hole development was found to be intermediate due to physical contact of the drill flutes around the internal drilled hole surface. Thus, rms torque was almost found to be the same. The reason was the chip removal operation through the flutes continued in this phase. The duration of this phase was within 3–5 s. The push-out delamination on the exit surface of the laminate was found to have occurred in this stage. However, the exit delamination was not relatively significant than pull-up delamination on the top surface of the work due to meager axial thrust force. The rms axial thrust was significantly reduced (83.2%) in this phase, as shown in Figure 5.

Phase VII over travel of drill after hole generation

In this phase, the drill bit travels without any chip generation as per approach length after the through-hole development. Thus, the machining torque, as well as axial thrust, was found to be constant at minimal state. The secondary and tertiary cutting edges (flutes) are still in touch with the work with the chip movement through the flutes. Thus, the rms torque was slightly decreased (27.3%) without any change of rms axial thrust (Figure 5). The phase duration was about 4–6 s, as shown in Figure 4.

This preliminary time-domain analysis of axial thrust force with corresponding torque signals

(Expt. 1) indicated that the actual chip removal was found to have occurred from phases I–V of the drilling cycle. The ideal machining time was about 24.2 s at 1225 r/min tool rotational speed with a feed rate of 0.025 mm/rev considering approach length for respective drill point angle of 110°, which also concluded the same. Therefore, the first five phases have been considered for the hole quality monitoring. However, the statistical analysis (gross) has been processed considering the early four phases as the last phase was short duration without any major process features except sharp downfall or rise of thrust force or torque, respectively. The experimental results on sensor-based features along with each process output at respective process parametric conditions as per full factorial design of experiments (i.e. 27 numbers of experiments) with repeated experiments have been presented in Table 4. The center point experiment (i.e. drill point angle 118°, drill rotational speed 2250 r/min, and feed rate 0.05 mm/rev) has been repeated twice (Expt. 28 and Expt. 29) to check the repeatability of the drilling machine.

Effect of process parameters on thrust force and torque

In this work, the first parametric interaction effect on rms and peak value of axial thrust with associated torque has been studied. Then, this parametric effect on each drilled hole quality feature, such as delamination, roughness, and cylindricity, has also been investigated to find the correlation between process outputs with sensor-based features. Finally, an attempt has been made to monitor the drilled hole quality using the raw signals of thrust force and torque as well as with their phase-wise rms values to discretize sound quality hole from poor hole quality. The response surface regression methodology has also been used to compare the monitoring capability considering different significant sensor-based strategies using peak and rms value of axial thrust and torque with respective process parametric settings.

The influence of process variables on the axial thrust force has been presented in Figure 6. The variation of the rms, as well as the peak value of thrust and torque, is indicated using the bar chart as shown. The rms and peak thrust force were found to be increased with an increase of feed rate keeping tool rotational speed and drill point angle constant. However, the peak thrust force variation was significant in the case of higher tool rotational speeds using a high drill point angle (128°) as shown. The effect of the drill point angle on thrust force was similar to with feed rate. But, this variation was found to be mitigated. There was a slight increase of peak thrust with a rise in tool rotational speed at high feed rate with a high drill point angle, which was found to be almost the same in case of other drilling conditions. Therefore, it may be concluded that the feed rate and

Table 4. Drilling input parameters and seven performance characteristics.

Expt. no.	Ø	N	F	F_z (rms)	F_z (peak)	T_z (rms)	T_z (peak)	F_d	R_z	C
1	110	1225	0.025	22.101	37.689	0.469	1.136	1.094	11.046	6.265
2	110	1225	0.05	28.148	48.860	0.729	1.612	1.106	11.552	6.445
3	110	1225	0.075	35.670	61.493	0.986	2.149	1.125	11.737	6.780
4	110	2250	0.025	21.476	38.147	0.729	1.577	1.087	9.956	6.077
5	110	2250	0.05	29.242	49.400	0.745	1.745	1.108	10.994	6.129
6	110	2250	0.075	35.847	57.869	0.966	2.024	1.120	11.311	6.489
7	110	3200	0.025	27.018	42.725	0.461	1.074	1.075	9.959	6.016
8	110	3200	0.05	29.957	48.599	0.549	1.353	1.102	10.638	6.164
9	110	3200	0.075	38.461	60.539	0.966	2.116	1.120	11.118	6.295
10	118	1225	0.025	22.055	37.918	0.389	0.866	1.078	12.396	6.473
11	118	1225	0.05	32.347	52.071	0.390	0.854	1.110	12.787	6.626
12	118	1225	0.075	42.223	66.872	0.586	1.301	1.129	12.941	6.697
13	118	2250	0.025	23.437	42.267	0.675	1.459	1.098	11.287	6.599
14	118	2250	0.05	33.197	55.962	0.685	1.580	1.113	12.239	6.683
15	118	2250	0.075	39.323	68.703	0.740	1.895	1.132	12.418	6.965
16	118	3200	0.025	21.707	39.024	0.577	1.239	1.090	11.325	6.575
17	118	3200	0.05	29.466	51.765	0.633	1.447	1.109	11.929	6.657
18	118	3200	0.075	38.576	66.338	0.780	1.841	1.128	12.038	6.878
19	128	1225	0.025	26.411	43.793	0.766	1.728	1.100	12.449	6.697
20	128	1225	0.05	33.442	55.809	0.665	1.706	1.111	13.469	6.999
21	128	1225	0.075	39.328	69.695	0.647	1.797	1.124	13.599	7.281
22	128	2250	0.025	25.179	46.387	0.664	1.550	1.102	11.717	6.714
23	128	2250	0.05	35.665	68.703	0.726	1.656	1.134	12.610	6.715
24	128	2250	0.075	44.340	76.065	0.833	1.931	1.142	12.748	7.017
25	128	3200	0.025	24.460	42.114	0.687	1.655	1.101	11.823	6.525
26	128	3200	0.05	39.542	69.733	0.550	1.284	1.136	12.207	6.636
27	128	3200	0.075	45.867	81.596	0.661	1.659	1.147	12.315	6.698
28	118	2250	0.05	33.200	45.162	0.688	1.680	1.114	12.242	6.673
29	118	2250	0.05	32.897	72.916	0.678	1.738	1.113	12.231	6.701
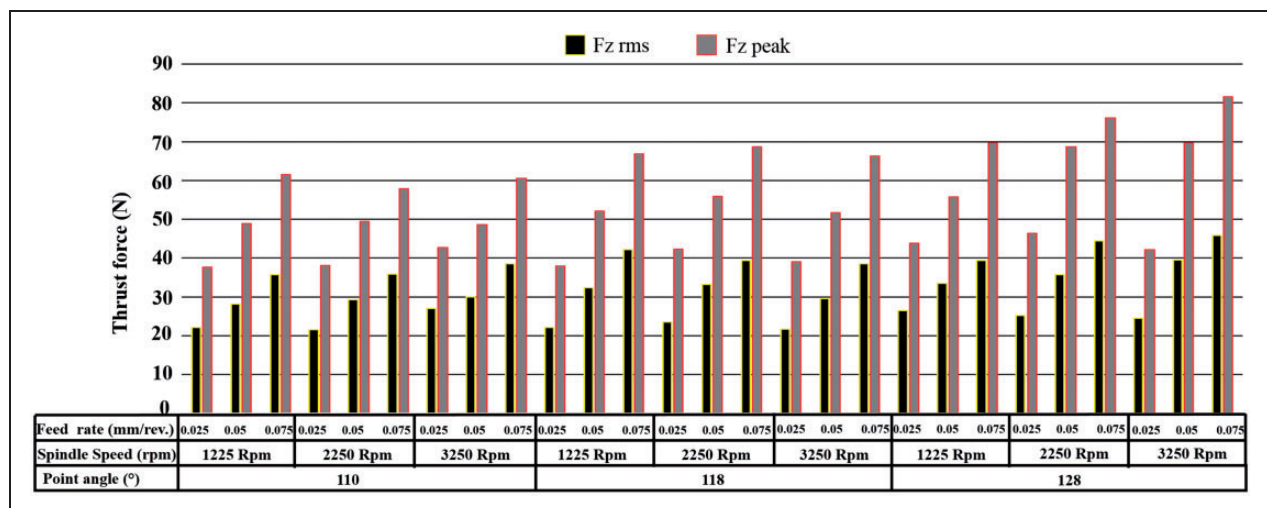
Figure 6. Variation thrust force with process parameters.

drill point angle were significant parameters on thrust force generation in drilling. The average value of rms and peak axial thrust force has been processed using different drill point angles. The mean rms (29.8, 31.4, and 34.9 N, respectively) and mean peak thrust force (49.5, 53.4, and 61.5 N, respectively) increased with an increase of point angle, which was more pronounced using high drill point angle (128°). However, the deviation of the peak to rms thrust value was found to be almost proportionally increased (40, 43, and 44%, respectively) with higher drill point angles.

The parametric effect on torque generation using rms and peak values has been presented in Figure 7. The rms torque was found to be increased with an increase of feed rate in most of the cases except with drill having a high point angle (128°). It was slightly reduced or little reduction followed by a slight increase at low or high tool rotational speeds (1225 and 3250 r/min), respectively. This irregular behavior was also noticed for peak torque generation as shown. The mean rms (0.73, 0.61, and 0.69 Nm, respectively) as well as average peak (1.64, 1.39, and 1.66 Nm, respectively) was found to be reduced with an increase of point angle followed by an enhancement using high point angle (128°). However, the deviation of the peak to rms thrust value was found to be reduced linearly (55.8, 55.9, and 58.5%, respectively) with a higher

drill point angle, i.e. completely reversed relative to axial thrust variation. Therefore, it may be concluded that higher axial thrust variation was compensated by an adequate reduction in torque fluctuation to maintain the stability of drilling operation.

Effect of process variables on hole quality

The second-order regression models have been developed for each drilled hole quality feature, namely delamination (F_d), surface roughness (R_z), and circularity error (C) in equations (3) to (5) using response surface methodology as lower-order polynomials were found to be inadequate. The adequacy of these models has been checked using the ANOVA table. The summarized major model competence parameters such as P-value, F-value, and R-square value of each model have been presented in Table 5. The lack-of-fit of these models has also been tested using corresponding P-value and F-value as shown. The P-value was found to be significant (less than 0.05) at a 95% confidence level for each model. The F-value of all the models developed was more than standard tabulated F-value at corresponding degrees of freedom of the model and residual error. The R-square value was well above 85% indicated a high degree of fitness of all the models. The adjusted R-square value was also
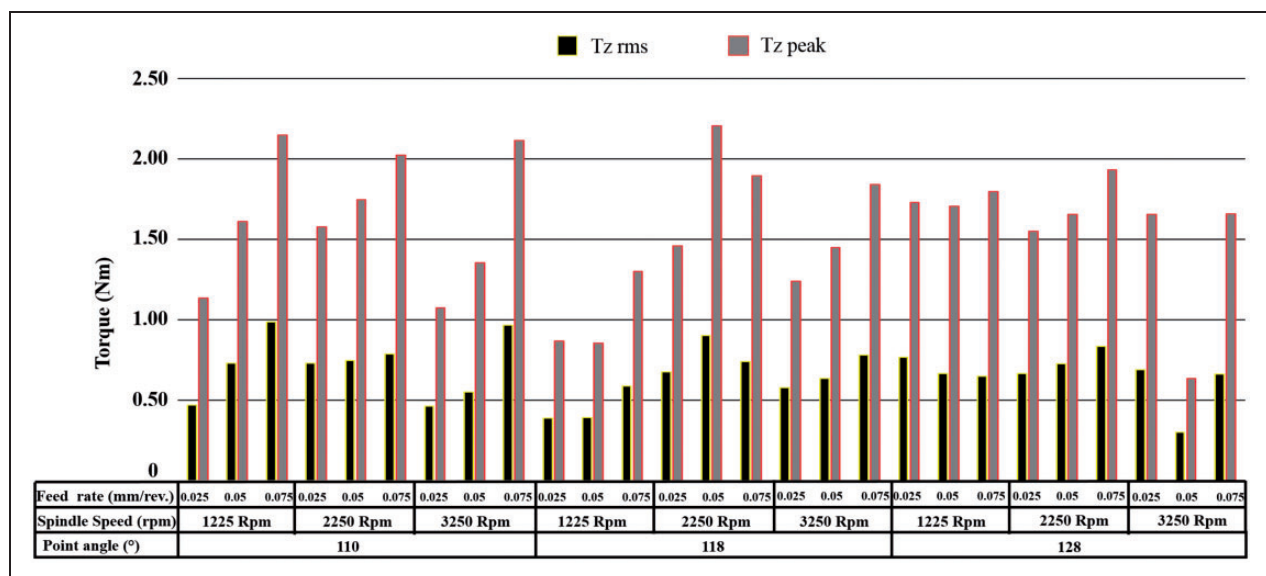
Figure 7. Variation of torque with process parameters.

Table 5. Summarized ANOVA table of hole quality models.

Process outputs	Lack-of-fit		Model					
	F-value (std F value)	P-value	R^2 (%)	R^2 (adj) (%)	F-value (std F value)	P-Value	Remarks
F_d	81.17 (2.31)	0.012	95.03	92.67	40.34 (3.18)	0.000	Significant
R_z	865.48 (2.31)	0.001	97.88	96.87	97.4 (3.18)	0.000	Significant
C	94.11 (2.31)	0.011	86.63	80.30	13.68 (3.18)	0.000	Significant

found to be close to the respective R-square value indicated the same. Therefore, each process output model was found to be highly adequate to represent the process characteristics that can be further used for the parametric influence on drilled hole quality. The lack-of-fit of the models has also found to be adequately qualified in the P-test and F-test at a 95% confidence level as indicated. Thus, insignificant coefficients were not necessarily to be omitted in revised regression models in the present case[37]

$$F_d = 1.582 - 0.00839\,Ø - 0.000067\,N + 1.133\,f \\ + 0.000033\,Ø^2 - 5.44\,f^2 + 0.000001\,Ø*N \\ + 0.000077\,N*f \tag{3}$$

$$R_z = -92.4 + 1.653\,Ø - 0.000929\,N + 83.4\,f \\ - 0.006480\,Ø^2 - 435.7\,f^2 - 0.000005\,Ø*N \\ - 0.181\,Ø*f + 0.00002\,N*f \tag{4}$$

$$C = -26.89 + 0.526\,Ø + 0.000271\,N + 9.4\,f \\ - 0.002063\,Ø^2 + 74.7\,f^2 - 0.000002\,Ø*N \\ - 0.047\,Ø*f - 0.00191\,N*f \tag{5}$$

The interaction effect of drill rotational speed and feed rate using different drill point angles on delamination, surface roughness, and circularity error of drilled hole have been presented in Figures 9 to 11, respectively, using 3D response surface plots as per equations (3) to (5).

The drilling-induced delamination was significantly increased with an increase of feed rate, which was more pronounced at higher drill spindle revolutions per minute using any drill point angle, as shown in Figure 8. It was increased (2.8, 2.9, and 4.2%, respectively) with the variation of feed rate from 0.025 to 0.075 mm/rev at low drill spindle speed 1225 r/min to high 3250 r/min. It was primarily due to greater drill thrust force at higher feed rate.[38] However, the influence of drill revolutions per minute was not so predominant on delamination. It was slightly increased and after that reduced with an increase of drill rotational speed except at a very high feed rate using a high drill point angle (128°) where delamination was increased sharply as shown. The average value of delamination considering all drilling experiments was found to be increased (1.1, 1.11, and 1.12, respectively) with an increase of drill point angle from 110° to 128° due to higher axial thrust development. Therefore, the feed rate was the most significant parameter on surface delamination using specific drill geometry. The worst drilled hole affected by delamination along with the best one having minimum delamination for each drill point angle has been presented using the optical macrograph in Figure 9. These drilled hole macrographs characterized the hole edge qualities such as fiber pull out.

The delamination factor has been calculated from the delamination area and nominal area of these images using "Image J software." It was found that the drilled hole damage was found to be less at lower feed rate with higher spindle speed using a low drill point angle (110°) in Expt. 7. However, it was found to be minimum at both low spindle revolutions minute and feed rate using a higher drill point angle (Expt. 10 and 19). The delamination factor was more significant considering the higher drill point angle though fiber pullout was not so predominant at these drilling conditions as shown. The fiber pullout problem was found to be severe at a high feed rate (0.075 mm/rev), especially using a higher drill point angle. This drilling-induced defect was more pronounced at higher drill spindle speed for higher drill point angle and vice versa as shown. Therefore, a low feed rate, along with higher spindle speed using a smaller point angle, was the best possible combination to reduce delamination induced surface damage.

The surface roughness of the drilled hole increased sharply with an increase of feed rate like delamination using a low drill point angle, which was found to be
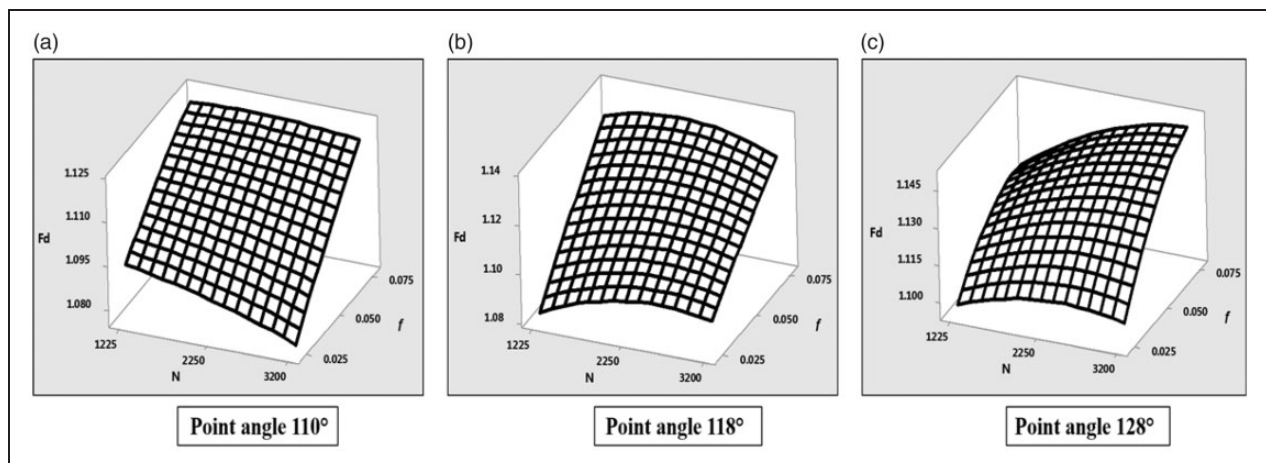
Figure 8. Interaction effect on delamination using drill point angle: (a) 110°, (b) 118°, and (c) 128°.
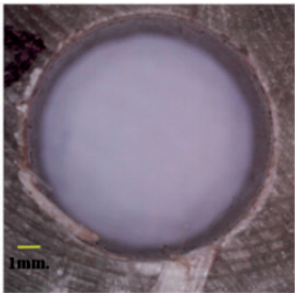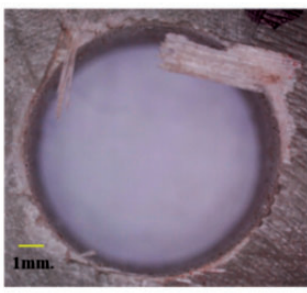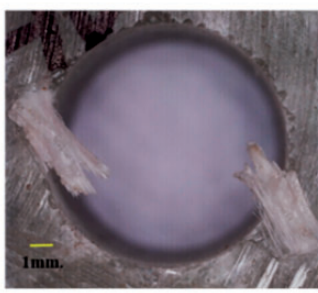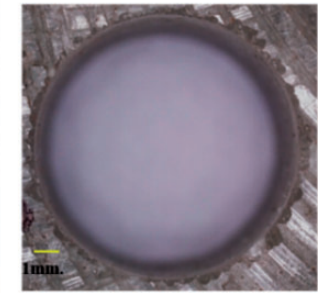
Figure 9. Maximum and minimum delaminated hole macrographs using different drill point angle.
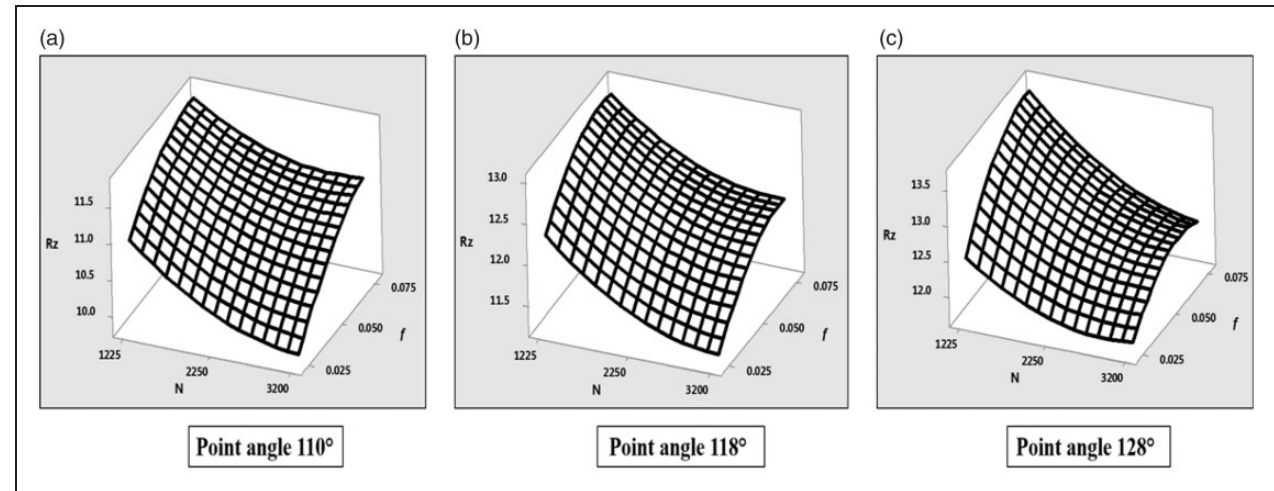
Figure 10. Interaction effect on roughness using drill point angle (a) 110°, (b) 118°, and (c) 128°.

stationary with a further increase of feed rate for higher drill point angle, as shown in Figure 10. On the other hand, the finish was drastically improved with a rise in drill spindle speed at a lower feed rate for each drill point angle, which was found to be stagnant at high feed rate using a low drill point angle. The average value of roughness considering all drilling experiments was found to be increased (10.9, 12.15, and 12.55 μm, respectively) with an increase of drill point angle from 110° to 128° due to lower torque development though the axial force was increased. Therefore, the internal surface roughness can be reduced at a lower feed rate with moderate spindle speed using a lower drill point angle.

The interaction effect of process variables on circularity error is specified as the radial distance between

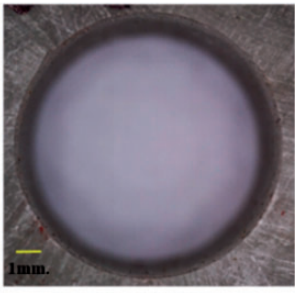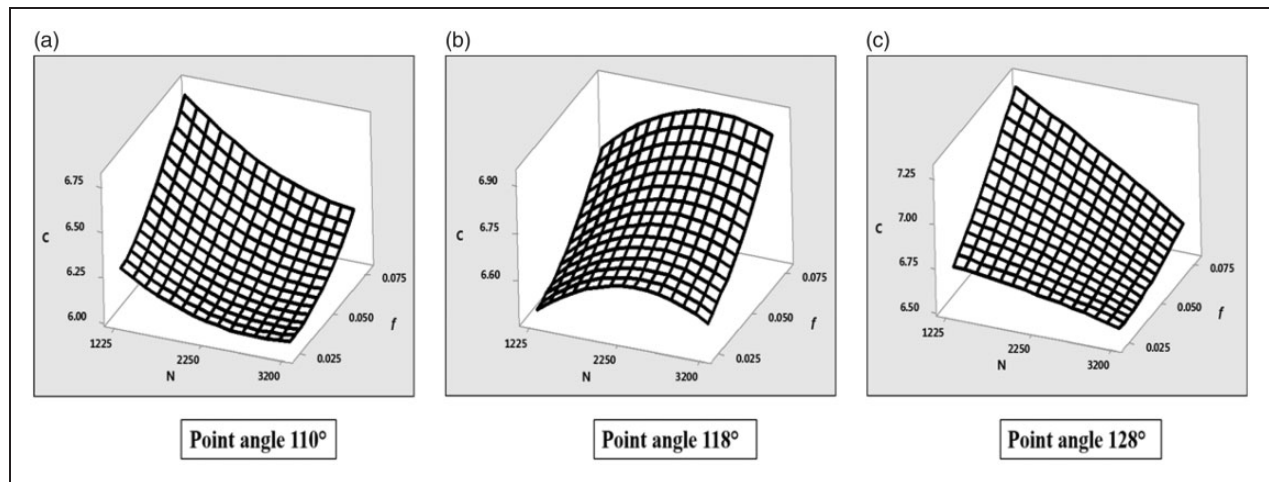**Figure 11.** Interaction effect on circularity using drill point angle: (a) 110°, (b) 118°, and (c) 128°.

two concentric circles separated by minimum possible distance, as illustrated in Figure 11 for each drill point angle. This macro deviation defect was also found to be less at a higher spindle speed with low feed rate as in case of surface roughness except for intermediate drill point angle 118° as shown. There was a sharp increase in roughness with an increase of feed rate like delamination, which was more predominant at low feed rate using any drill point angle. However, it was found to be improved at high drill spindle speed, especially with low feed rate conditions as shown. The average circularity error considering all the experiments was increased (6.31, 6.68, and 6.81 μm, respectively) with an increase of point angle from 110° to 128° due to reduction in torque development. Thus, the circularity error can be reduced at a lower feed rate with a higher spindle speed combined with a lower drill point angle.

Monitoring of hole quality in drilling

The hole surface characteristics have been studied with corresponding thrust and torque signals in drilling. The objective was to investigate the primary reason for the respective drilled hole quality. The defective drilled hole, as well as the best-drilled hole with respect to top surface delamination, roughness, and circularity error along with associated sensor signals, has been presented. Various global statistical parameters, such as mean, standard deviation, and rms, as well as a local parameter like peak have been considered in this investigation. These statistical variables have been calculated for each significant phase (phases I–IV) of the drilling cycle to compare the deviations. After that, a sensitivity analysis of statistical parameters of thrust and torque signals in different drilling phases has also been processed. Finally, an attempt has been made to improve the predictability of each developed hole quality feature regression model using significant sensor-based features with process variables.

Study on surface delamination using sensors' signals

The CFRP laminates were found to be significantly affected by drilling process parameters due to delamination on the top surface. It was mainly characterized by fiber pullout along with piles of damage around the drilled hole periphery. It was more pronounced at a higher feed rate using a higher drill point angle, as shown in Figure 12 (Expt. 27) with the highest delamination error (1.147). The primary reason was higher axial thrust force (peak as well as rms value) development with significant fluctuation (%) evidenced by higher standard deviation during phases I and II in the drilling cycle as shown. Thus, the torque requirement was also found to be higher to maintain stability during drilling. However, the drilling torque also found to be highly fluctuated with respect to mean torque, especially in phases II and IV. Therefore, the internal surface roughness was reduced (12.32 μm) with predominant circularity error (6.7 μm) in this parametric conditions.

The surface delamination was found to be reduced significantly (1.075) without any fiber pullout at a lower feed rate with higher tool rotational speed using a low point angle drill, as shown in Figure 13 (Expt. 7). The rms value of axial thrust force, as well as torque, was lower (44.7% and 30.3%, respectively) than the previous condition (Table 3). The fluctuation of axial force significantly decreased (67.3%) with a corresponding reduction in torque variation (30.5%) concerning rms value as indicated, which was more pronounced in phases I and II, respectively. The peak axial force was found to be reduced from 81.6 to 42.72 N with associated peak torque reduction (1.66–1.06 Nm). Thus, the surface roughness (9.959 μm) and circularity error (6.016 μm) were also found to be improved at this parametric condition due to a more uniform torque. Therefore, the axial thrust force was a prime indicator of surface delamination.
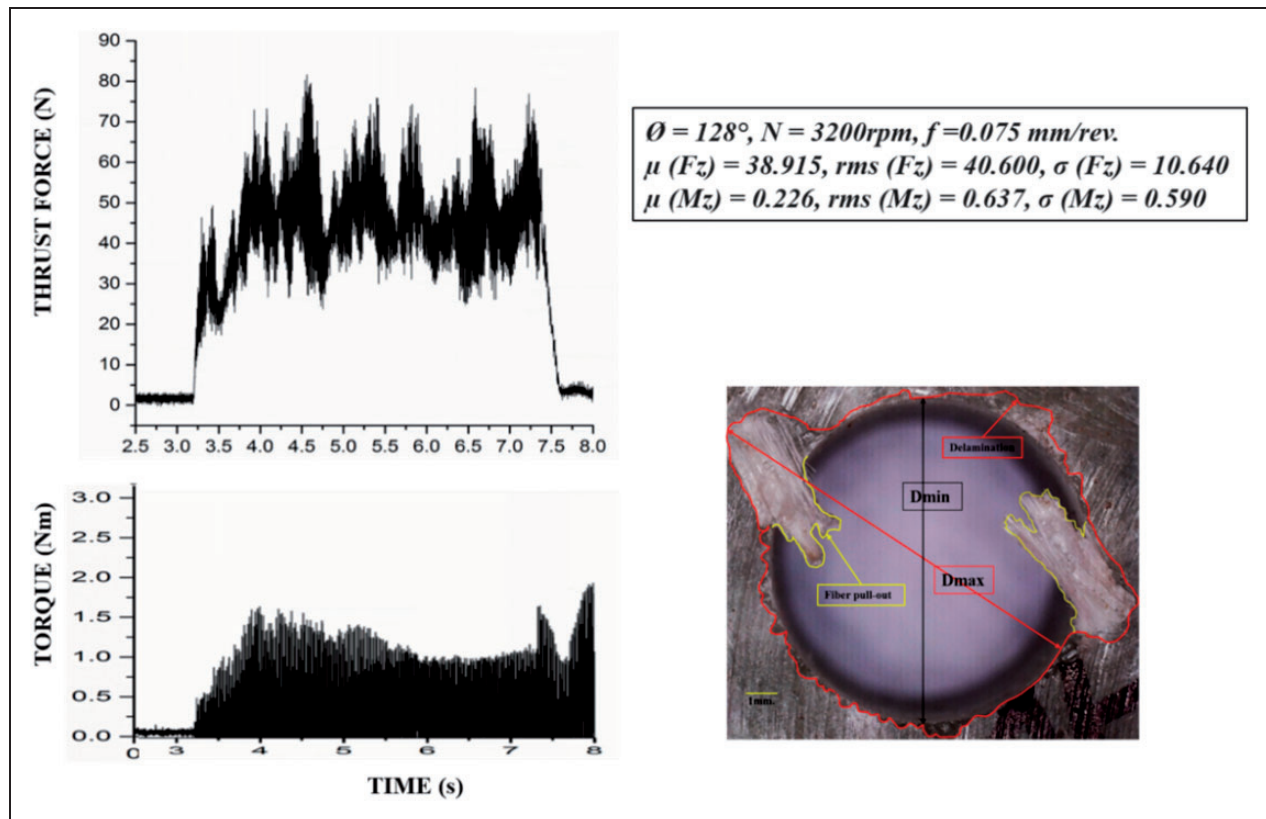
Figure 12. Maximum delaminated hole macrograph with corresponding thrust and torque signals (Expt. 27).

Study on surface roughness using sensors' signals

The surface roughness of the drill hole was found to be maximum (13.6 μm) at a higher feed rate with lower drill spindle revolutions per minute using a higher point angle drill (Expt. 21). The axial thrust force and torque signals with corresponding roughness profile (cut-off length of 3.5 mm from both sides along with the working thickness, i.e. 70% of total work thickness) have been presented in Figure 14. However, the average roughness has been calculated considering several passes at different zones of internal drilled hole surface during roughness test. The mean, rms, and peak as well as standard deviation of axial force were relatively higher at phases III and IV rather than the initial phases of drilling cycle. Thus, the average torque was higher in the last phases. The delamination (1.13 μm) and circularity error (7.28 μm) were also found to be higher due to the same reasons. So, the internal surface finishes highly influenced due to high axial force and its deviation along with higher torque development in this condition. However, the roughness profile was comprised of significant fluctuation at multiple points (troughs) at regular intervals, which were found to be substantial during intermediate phases and drastically diminished during the final phases in the drilling cycle (i.e. toward the bottom side of the drilled hole as shown). Thus, the torque fluctuation during initial

phases with several peaks was found to be extensively reduced in the final drilling phases due to a fully loaded drill in these phases. However, the axial force was fluctuated because of obstruction on drill feeding loaded by the machined chips in the last phases as shown.

The surface finish was found to be improved ($R_z = 9.96 \mu$m) at a low feed rate (0.025 mm/rev) with medium tool rotational speed using a low drill point angle (Expt. 4). The roughness profile having a 3.5 cut-off length on both sides through the drilled hole depth with corresponding axial thrust force and torque signals has been illustrated in Figure 15. The mean as well as rms axial force was decreased significantly (40.2 and 45.4%) than the previous condition without any variation of its fluctuation, which was more predominant in phases III and IV. However, the rms torque was found to be slightly increased (12.3%) due to more variation of torque. The rms and mean torque were marginally higher in phases II and III. The peak thrust force was reduced from 69.7 to 38.2 N without much variation of peak torque. Thus, the roughness profile was much smoother with two to three non-uniform troughs during intermediate phases in the drilling cycle with significant fluctuation in drilling torque as shown. The roughness profile was found to be smoother evidenced by uniform torque profile during the final phases. However, the axial thrust force was found to be fluctuated as soon as the drill lips peeps out of the workpiece. The
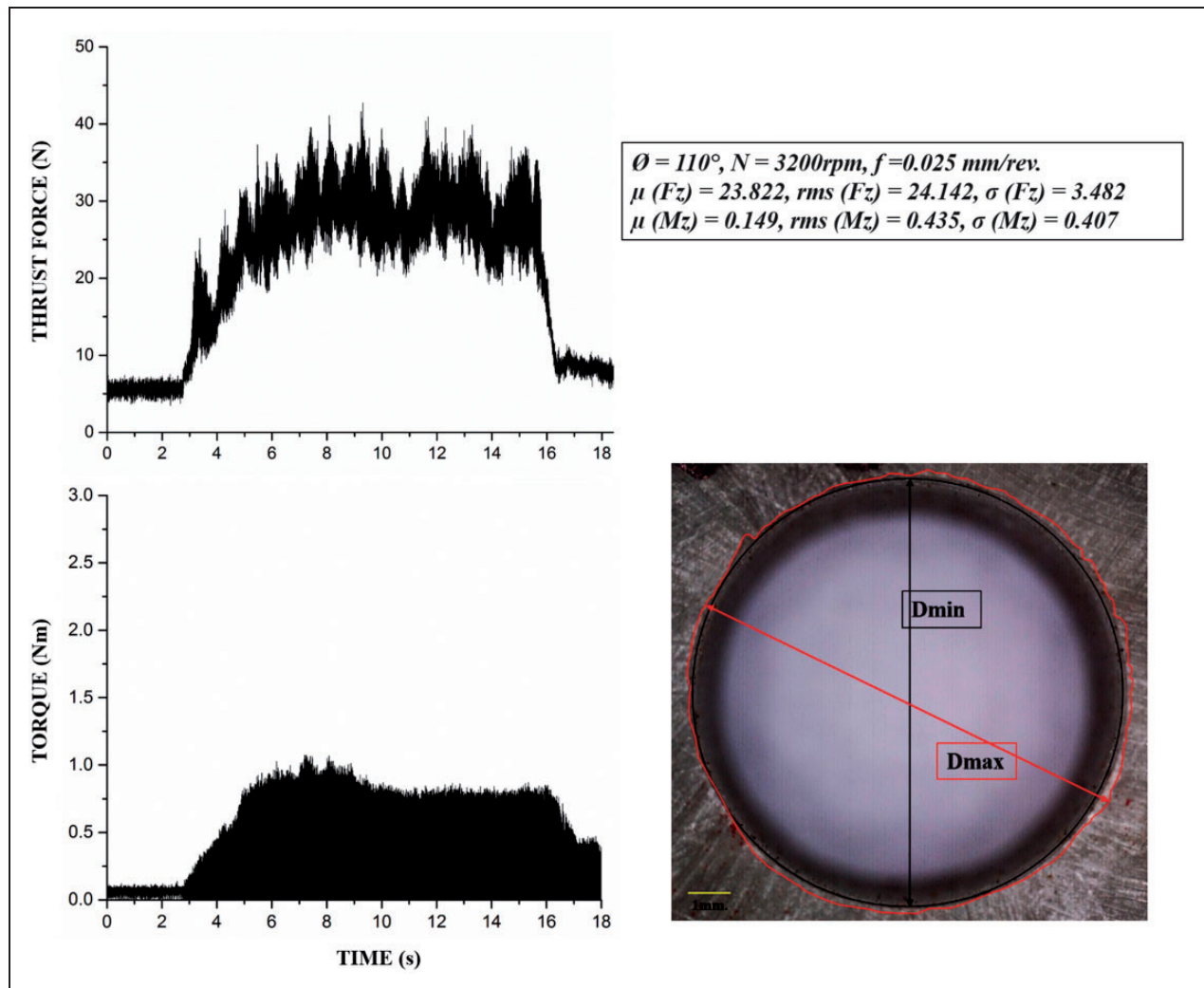
Figure 13. Minimum-delaminated hole macrograph with corresponding thrust and torque signals (Expt. 7).
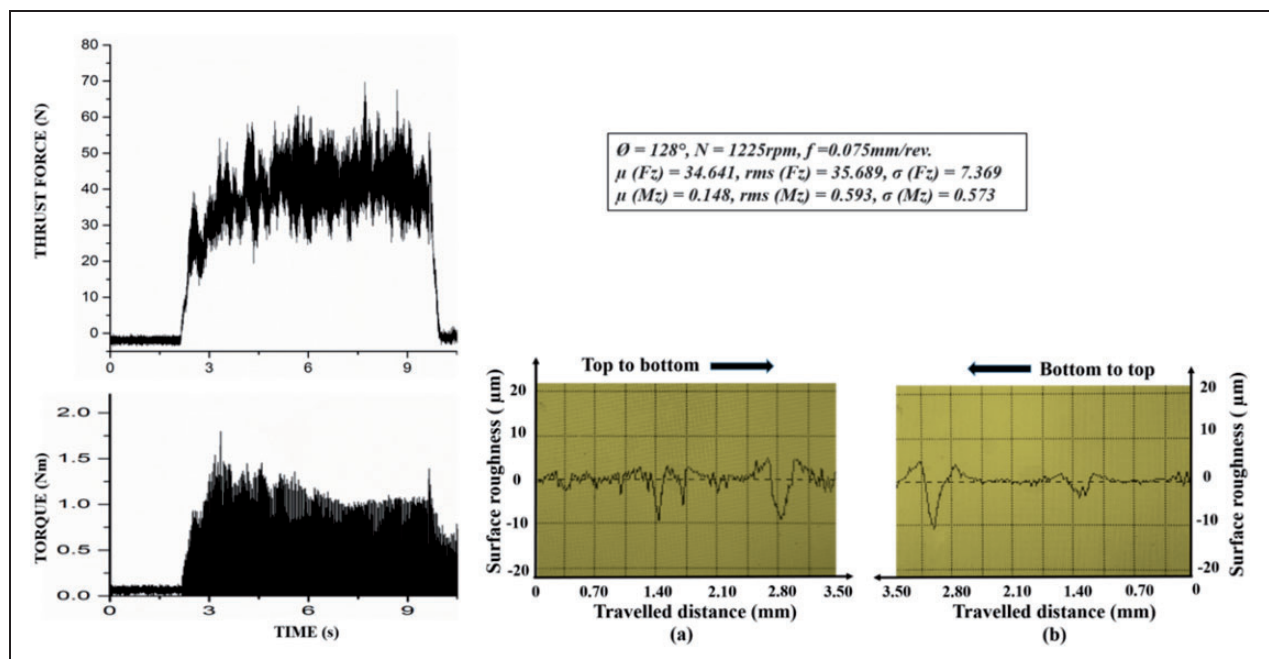
Figure 14. Maximum rough hole profile with thrust and torque signals (Expt. 21).
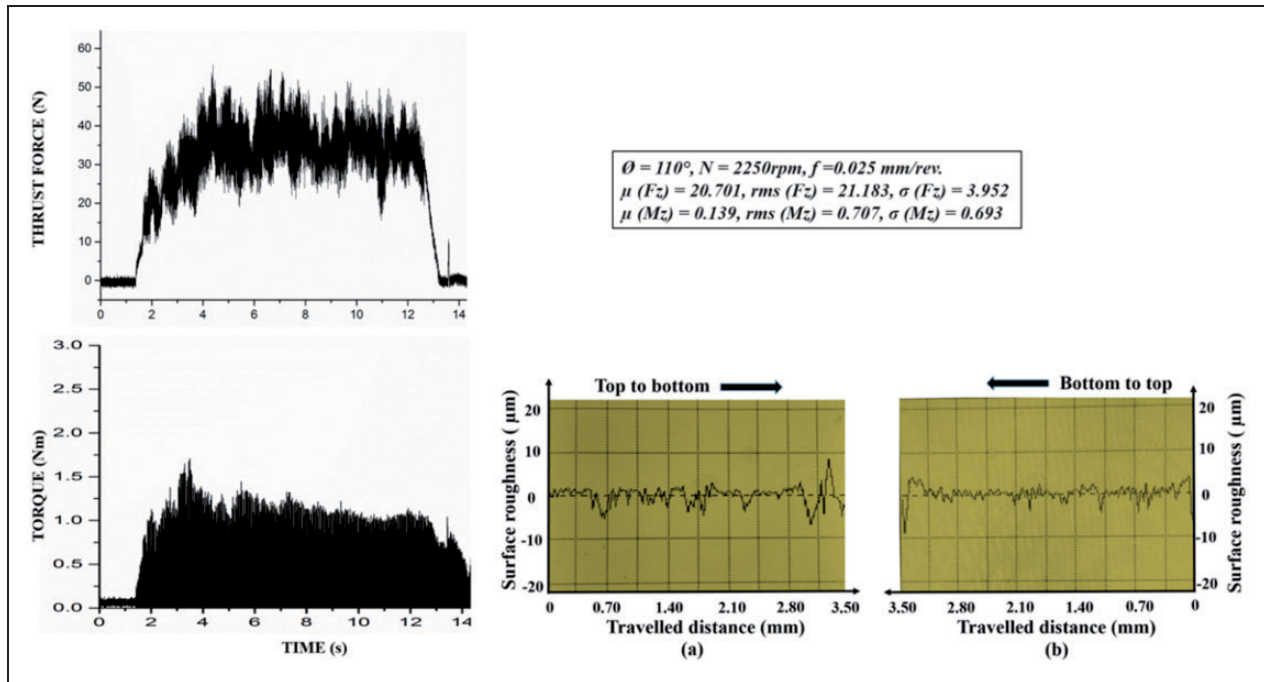
Figure 15. Minimum rough hole profile with corresponding thrust and torque signals (Expt. 4).
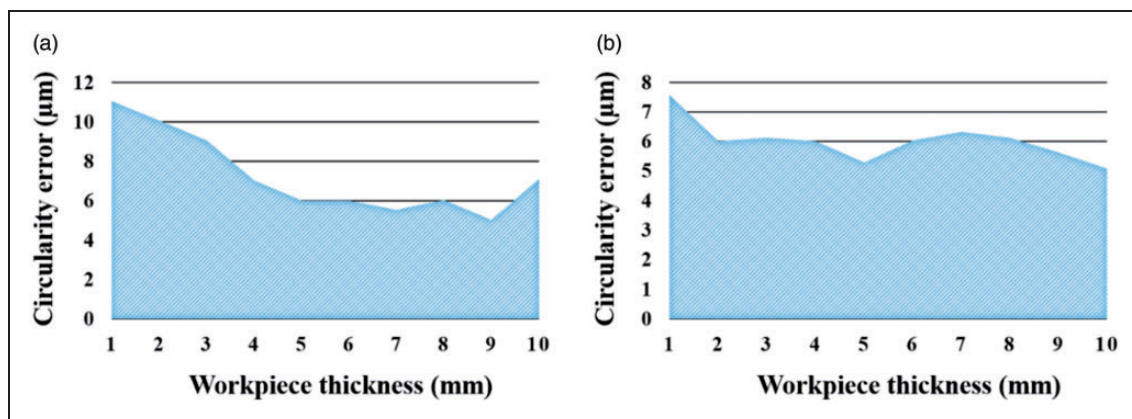
Figure 16. Variation of circularity profile through the drilled hole depth for maximum (Expt. 21) and (b) minimum (Expt. 7) mean circularity error.

delamination problem (1.087 μm) and circularity error (6.08 μm) were both improved due to low axial thrust. Thus, an average axial force was a better predictor than its deviation, especially the last two phases rather than initial phases as found in case of maximum delamination.

Study on circularity error using sensors' signals

The circularity is a circumferential defect related to surface waviness rather than roughness. However, the circularity error was also found to be maximum (7.281 μm) at a higher feed rate with lower drill spindle revolutions per minute using a higher point angle drill (Expt. 21), i.e. same parametric condition for the highest surface roughness. The thrust

force with associated torque signals along with circularity variation profile along the drilled hole depth has been presented in Figures 14 and 16, respectively. It was primarily due to higher thrust as well as higher torque along with higher fluctuations of each, which resulted in non-uniform process variations. Thus, the circularity error was found to be non-uniform through the drilled hole though there was significant improvement during the final phases in the drilling cycle, as indicated in Figure 16(a). However, the mean circularity error was considerably improved at the same parametric conditions as found in case of minimum delamination (i.e. low feed rate with high drill rotational speed using low drill point angle) at Expt. 7. The delamination error was also found to be minimum (1.075 μm) at this parametric setting. The

Table 6. Variation of statistical parametric features of thrust and torque for delamination.

Drill point angle of 110°

| | #3 F_d (Worse) F_z | | | | #7 F_d (Best) F_z | | | | | | | | #3 F_d (Worse) M_z | | | | #7 F_d (Best) M_z | | | | | | | |
	μ	rms	σ	P	μ	rms	σ	P	$\Delta\mu$	Δrms	$\Delta\sigma$	ΔP	μ	rms	σ	P	μ	rms	σ	P	$\Delta\mu$	Δrms	$\Delta\sigma$	ΔP
S	32.4	35.7	5.1	61.5	23.8	27.0	3.5	42.7	0.36	0.32	0.46	0.44	0.23	0.99	0.99	2.15	0.15	0.46	0.41	1.07	0.52	1.14	1.42	1.00
S1	21.7	22.9	7.4	38.7	14.4	15.1	4.7	28.9	0.51	0.52	0.57	0.34	0.16	0.78	0.76	2.00	0.06	0.25	0.24	0.74	1.52	2.19	2.23	1.69
S2	33.0	33.3	4.7	47.4	25.4	25.6	3.2	37.3	0.30	0.30	0.45	0.27	0.16	1.15	1.14	2.02	0.15	0.53	0.51	1.07	0.03	1.18	1.25	0.88
S3	36.3	36.5	3.5	46.1	26.5	26.7	2.5	35.1	0.37	0.37	0.38	0.31	0.20	1.15	1.14	2.06	0.17	0.51	0.48	1.01	0.12	1.27	1.39	1.03
S4	38.5	38.8	4.9	61.5	29.0	29.2	3.5	42.7	0.33	0.33	0.39	0.44	0.39	0.98	0.90	2.15	0.21	0.46	0.41	0.87	0.91	1.14	1.20	1.47

Drill point angle of 118°

| | #15 F_d (Worse) F_z | | | | #10 F_d (Best) F_z | | | | | | | | #15 F_d (Worse) M_z | | | | #10 F_d (Best) M_z | | | | | | | |
	μ	rms	σ	P	μ	rms	σ	P	$\Delta\mu$	Δrms	$\Delta\sigma$	ΔP	μ	rms	σ	P	μ	rms	σ	P	$\Delta\mu$	Δrms	$\Delta\sigma$	ΔP
S	37.4	39.3	7.2	68.7	20.6	22.1	3.8	37.9	0.82	0.78	0.88	0.81	0.24	0.74	0.69	1.89	0.16	0.39	0.32	0.87	0.49	0.90	1.18	1.19
S1	38.7	40.1	10.6	68.7	12.0	13.1	5.2	29.5	2.22	2.06	1.03	1.33	0.12	0.48	0.47	1.22	0.09	0.20	0.17	0.56	0.34	1.46	1.70	1.18
S2	32.6	33.1	5.9	50.8	21.9	22.2	3.3	33.3	0.49	0.49	0.79	0.53	0.17	0.83	0.82	1.56	0.15	0.39	0.36	0.85	0.18	1.13	1.25	0.84
S3	36.2	36.7	6.1	51.4	25.3	25.6	3.8	37.9	0.43	0.43	0.61	0.36	0.28	0.70	0.84	1.87	0.20	0.44	0.39	0.87	0.39	0.59	1.13	1.16
S4	42.2	42.7	6.3	68.7	23.1	23.3	3.0	37.0	0.82	0.83	1.08	0.86	0.38	0.75	0.64	1.89	0.20	0.40	0.34	0.87	0.88	0.89	0.90	1.18

Drill point angle of 128°

| | #27 F_d (Worse) F_z | | | | #19 F_d (Best) F_z | | | | | | | | #27 F_d (Worse) M_z | | | | #19 F_d (Best) M_z | | | | | | | |
	μ	rms	σ	P	μ	rms	σ	P	$\Delta\mu$	Δrms	$\Delta\sigma$	ΔP	μ	rms	σ	P	μ	rms	σ	P	$\Delta\mu$	Δrms	$\Delta\sigma$	ΔP
S	38.9	45.9	10.6	81.6	23.0	26.4	5.1	43.8	0.69	0.74	1.10	0.86	0.23	0.66	0.59	1.66	0.10	0.77	0.74	1.73	1.29	−0.14	−0.21	−0.04
S1	22.5	25.8	12.6	49.2	13.0	14.5	6.5	31.9	0.73	0.77	0.94	0.54	0.06	0.43	0.42	1.02	0.06	0.51	0.50	1.48	0.05	−0.16	−0.16	−0.31
S2	39.6	41.4	11.8	72.9	22.9	23.3	4.3	36.6	0.73	0.77	1.72	0.99	0.21	0.76	0.73	1.66	0.17	0.87	0.85	1.73	0.22	−0.13	−0.15	−0.04
S3	46.7	47.5	8.8	73.2	28.5	28.9	4.7	43.8	0.64	0.64	0.88	0.67	0.32	0.71	0.64	1.63	0.01	0.86	0.86	1.27	23.8	−0.18	−0.26	0.28
S4	46.8	47.7	9.3	81.6	27.6	28.0	4.7	43.4	0.70	0.71	0.97	0.88	0.32	0.66	0.58	1.66	0.15	0.76	0.75	1.50	1.07	−0.14	−0.23	0.11

thrust force signal with corresponding torque signal and circularity variation profile through the hole depth have been shown in Figures 13 and 16, respectively. The rms value of thrust and torque was reduced almost the same rate (31.3 and 29.1%, respectively) along with slight improvement in standard deviation or fluctuation of each (5.8 and 28.1%, respectively). There was little improvement in circularity error just after the initiation of the drilling operation, which again found to deteriorate toward the last phases in the drilling cycle, as shown in Figure 16(b). However, the drilled hole may be characterized by almost uniform as well as less circularity throughout the drilling hole (cycle). The internal surface roughness (9.96 μm) was also found to be less as expected. Thus, here, the circularity error was strongly inversely correlated with axial thrust force as well as torque development.

Sensitivity analysis of sensors' based features

In this work, three-time domain global (mean, rms, and standard deviation) and one local (peak) statistical parameters on thrust force and torque signals have been considered to investigate the correlation with drilled hole quality features (delamination, roughness, and circularity). These signal-based statistical characteristics for the worst drilled hole as per delamination defect has been compared with the best-drilled hole using each drill bit having different point angle (110°, 118°, and 128°). The mean, rms, standard deviation, and peak value of corresponding thrust force and torque signals of each significant phase (phases I–IV) have also been processed, as shown in Table 6.

The percent deviation of each statistical parameter value between poor quality hole with an excellent drilled hole has been presented to compare the correlation with delamination related defects. For example, Expt. 3 and Expt. 7 were found to be the worst (maximum delamination) and the best (minimum delamination) drilled a hole using a 110° point angle drill.

Thus, the thrust force and torque signals of theses two drilling experiments have been divided into phases, as discussed earlier. Then, the statistical parameters' values have been determined for phases I–IV as well as total phases I–IV for these two experiments thrust force and torque signals, as indicated in table. Thus, the analysis has been continued for other drill point angles in the same way. The result suggested that the average percent deviation of thrust force was found to be higher (81.6%) for standard deviation, which was more pronounced with a higher drill point angle (46.4, 88.4, and 110%, respectively) as indicated. The maximum average difference was also found to be higher (79.9%) for the standard deviation of torque signals. However, this deviation for torque was found to be diminished or even inverted with an increase of drill point angle (142%, 118.3%, and −21%) to maintain the process stability during drilling. However, the average percent deviation for peak thrust (70.5%) as well as peak torque (71.4%) was also higher than the mean or rms axial thrust. Therefore, it may be concluded that fluctuation of axial thrust and torque was strongly correlated with the degree of surface delamination of drilled CFRP composite laminated hole. The variation of standard deviation from phases I–IV in the drilling cycle for thrust force and torque has been presented in Figure 17(a) and (b), respectively. The standard deviation of thrust force in phases I and II was found to be higher for the highly delaminated hole indicated its capability to identify poorly drilled hole from a less delaminated hole (Figure 17(a)). However, this effect was also prominent in the case of torque except at low drill rotational speed using a high drill point angle (Expt. 19), as shown in Figure 17(b).

The sensitivity analysis has been extended to drilled hole surface roughness, as shown in Table 7. The average deviation of the mean value of thrust force (72.2%), as well as torque (63.1%), was found to be highly significant than other statistical parameters. The average deviation of rms (70.4%) followed by
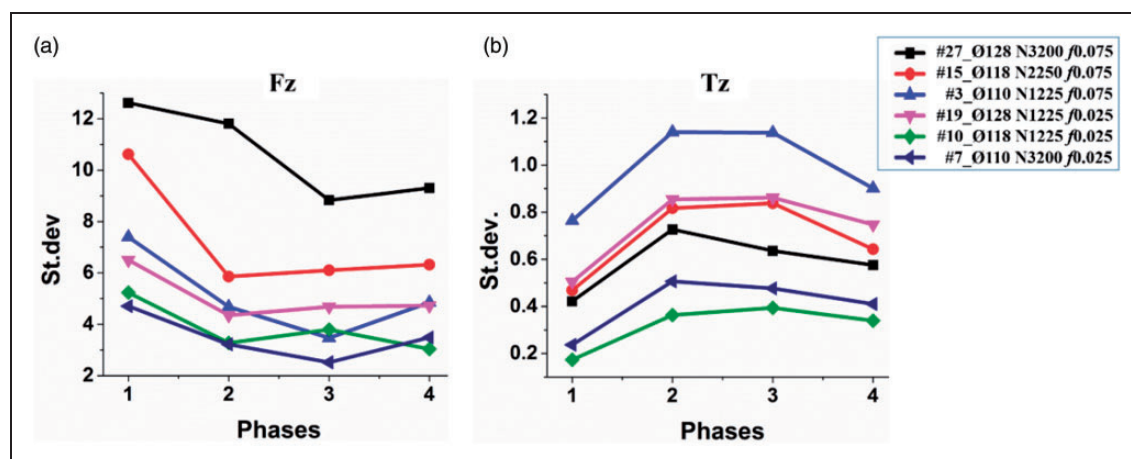
Figure 17. Variation of the standard deviation of (a) thrust and (b) torque for delamination.

Table 7. Variation of statistical parametric features of thrust and torque for roughness.

Drill point angle of 110°

| | #3 R_z (Worse) F_z | | | | #4 R_z (Best) F_z | | | | | | | | #3 R_z (Worse) M_z | | | | #4 R_z (Best) M_z | | | | | | | |
	μ	rms	σ	P	μ	rms	σ	P	$\Delta\mu$	Δrms	$\Delta\sigma$	ΔP	μ	rms	σ	P	μ	rms	σ	P	$\Delta\mu$	Δrms	$\Delta\sigma$	ΔP
S	32.4	35.7	5.1	61.5	20.7	21.5	4.0	38.1	0.56	0.66	0.29	0.61	0.23	0.99	0.99	2.15	0.14	0.73	0.69	1.58	0.64	0.35	0.42	0.36
S1	21.7	22.9	7.4	38.7	13.4	14.6	5.7	28.6	0.62	0.57	0.29	0.35	0.16	0.78	0.76	2.00	0.08	0.45	0.45	1.24	0.97	0.72	0.71	0.62
S2	33.0	33.3	4.7	47.4	22.5	22.8	4.1	38.0	0.47	0.46	0.16	0.25	0.16	1.15	1.14	2.02	0.14	0.83	0.82	1.58	0.16	0.39	0.40	0.28
S3	36.3	36.5	3.5	46.1	23.7	23.9	2.8	32.8	0.53	0.53	0.24	0.40	0.20	1.15	1.14	2.06	0.13	0.82	0.81	1.54	0.48	0.41	0.41	0.34
S4	38.5	38.8	4.9	61.5	23.2	23.5	3.2	38.1	0.66	0.65	0.51	0.61	0.39	0.98	0.90	2.15	0.20	0.73	0.70	1.48	0.92	0.35	0.29	0.45

Drill point angle of 118°

| | #12 R_z (Worse) F_z | | | | #13 R_z (Best) F_z | | | | | | | | #12 R_z (Worse) M_z | | | | #13 R_z (Best) M_z | | | | | | | |
	μ	rms	σ	P	μ	rms	σ	P	$\Delta\mu$	Δrms	$\Delta\sigma$	ΔP	μ	rms	σ	P	μ	rms	σ	P	$\Delta\mu$	Δrms	$\Delta\sigma$	ΔP
S	41.1	42.2	5.6	66.9	20.9	23.4	4.2	42.3	0.97	0.80	0.33	0.58	0.33	0.59	0.51	1.30	0.15	0.68	0.57	1.46	1.19	−0.13	−0.09	−0.11
S1	35.7	36.1	5.3	52.4	14.9	15.9	5.5	30.0	1.40	1.27	−0.03	0.75	0.27	0.66	0.60	1.26	0.08	0.32	0.32	0.78	2.62	1.04	0.91	0.63
S2	42.8	43.2	5.2	59.8	19.6	20.0	3.6	31.8	1.18	1.16	0.47	0.88	0.31	0.63	0.55	1.30	0.14	0.57	0.55	1.17	1.16	0.11	0.00	0.11
S3	43.7	44.0	5.7	59.4	24.8	25.1	3.5	37.1	0.76	0.76	0.63	0.60	0.37	0.61	0.48	1.27	0.17	0.73	0.71	1.29	1.15	−0.16	−0.32	−0.01
S4	42.4	42.8	6.1	66.9	24.2	24.5	4.3	42.3	0.75	0.74	0.44	0.58	0.35	0.55	0.42	1.10	0.21	0.72	0.69	1.46	0.71	−0.23	−0.39	−0.25

Drill point angle of 128°

| | #21 R_z (Worse) F_z | | | | #22 R_z (Best) F_z | | | | | | | | #21 R_z (Worse) M_z | | | | #22 R_z (Best) M_z | | | | | | | |
	μ	rms	σ	P	μ	rms	σ	P	$\Delta\mu$	Δrms	$\Delta\sigma$	P	μ	rms	σ	P	μ	rms	σ	P	$\Delta\mu$	Δrms	$\Delta\sigma$	P
S	34.6	39.3	7.4	69.7	21.2	25.2	5.5	46.4	0.63	0.56	0.35	0.50	0.15	0.65	0.57	1.80	0.14	0.66	0.59	1.55	0.06	−0.03	−0.03	0.16
S1	20.9	23.7	11.1	42.6	11.8	13.8	7.2	28.9	0.77	0.71	0.55	0.47	0.09	0.36	0.35	0.93	0.10	0.36	0.34	0.90	−0.10	0.01	0.02	0.04
S2	37.3	37.7	5.6	58.1	19.7	20.4	5.2	39.2	0.89	0.85	0.06	0.48	0.11	0.69	0.68	1.80	0.14	0.65	0.64	1.36	−0.18	0.05	0.06	0.32
S3	38.5	39.0	6.0	58.6	27.6	28.0	4.7	46.4	0.39	0.39	0.29	0.26	0.20	0.73	0.70	1.47	0.13	0.75	0.74	1.46	0.57	−0.03	−0.05	0.01
S4	41.9	42.4	6.8	69.7	25.8	26.2	4.7	43.8	0.62	0.62	0.43	0.59	0.19	0.60	0.56	1.39	0.20	0.67	0.64	1.55	−0.01	−0.11	−0.12	−0.10

peak (56.5%) thrust was also competitive with mean value as indicated. However, the average variation of both mean thrust and mean torque was higher (97 and 119%, respectively) using an intermediate 118° drill point angle. Thus, the mean value of thrust and torque was a prime indicator of the internal surface roughness of the CFRP composite-laminated drilled hole.

The variation of mean thrust and torque from the drilling phases I–IV has been illustrated in Figure 18. There were two separate clusters of thrust force data related to a rough drilled hole (high mean thrust) from an excellent finished hole (low mean thrust), as shown in Figure 18(a). It was not so prominent, especially using a higher drill point angle without any significant cluster of data for torque signal as shown. However, the prediction of drilled hole quality was found to be improved considering phase III in the drilling cycle where mean torque value was higher for rough hole surface and lower for finer hole surface, as shown in Figure 18(b).

The average deviation of peak, mean, rms, and standard deviation of axial thrust force was found to be almost the same (64, 60, 59, and 57%, respectively). However, the average variation of the standard deviation of torque (81%) was higher than the peak (76%) and rms (70%) without a significant deviation of the mean. Thus, peak thrust force with torque fluctuation was a primary indicator of circularity error of CFRP-laminated drilled hole. The peak thrust force deviation was higher (81%) using intermediary drill point angle 118°, as found in case sensitivity analysis for surface roughness. However, the standard deviation of torque variation was drastically reduced or even reversed with a higher drill point angle (142%, 118%, and −18%), as indicated in Table 8.

The most significant peak thrust force and the standard deviation of torque in different drilling phases have been presented in Figure 19(a) and (b), respectively. The peak thrust force was comparatively higher for a high circularity error hole than more uniform with less circularity hole. The same phenomenon was also noticed for torque standard deviation except at high drill spindle rotational speed using a high drill point angle (Expt. 5), as shown in Figure 19(b). The peak thrust force was found to be maximum in phase IV of the drilling cycle, whereas the torque fluctuation was diminished indicated a fully loaded drill during this final phase.

The above sensitivity analysis of various statistical parameters (mean, standard deviation, rms, and peak) of thrust and torque during drilling indicated the most significant one for delamination, surface roughness, and circularity error. However, the overall average percent deviation of thrust force and torque was found to be higher with rms value (64.2%) and standard deviation (56.9%), respectively, considering all drilled hole quality features. The gross percent deviation (i.e. considering thrust and torque) was maximum using peak (58.6%) followed by rms (58.1%), mean (58%), and standard deviation (57%) value. Thus, local peak value was found to be slightly better than global rms considering both signals, whereas global rms and the standard deviation were a better indicator for the prediction of drilled hole quality. Therefore, the most significant local peak value and global rms have been further used as an input in the regression models of hole quality characteristics to check their degree of fitness as well as prediction error considering all the drilling experiments.

Monitoring of hole quality using sensors' signal-based strategies

The sensitivity analysis of the statistical parameters indicated that local peak and global rms value of thrust and torque in the drilling of CFRP laminate were the most significant indicator of drilled hole surface quality. Although global mean and standard deviation were also predominant in the prediction of
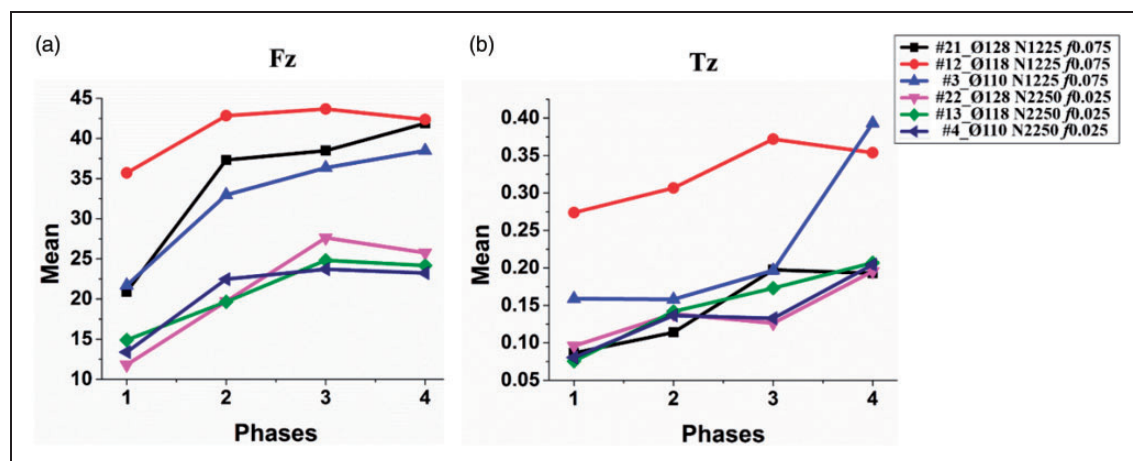

Figure 18. Variation of (a) mean thrust and (b) mean torque for roughness.

Table 8. Variation of statistical parametric features of thrust and torque for circularity.

Drill point angle of 110°

| | #3 C (Worse) F_z | | | | #7 C (Best) F_z | | | | | | | | #3 C (Worse) M_z | | | | #7 C (Best) M_z | | | | | | | |
	μ	rms	σ	P	μ	rms	σ	P	$\Delta\mu$	Δrms	$\Delta\sigma$	ΔP	μ	rms	σ	P	μ	rms	σ	P	$\Delta\mu$	Δrms	$\Delta\sigma$	ΔP
S	32.4	35.7	5.1	61.5	23.8	27.0	3.5	42.7	0.4	0.3	0.5	0.4	0.23	0.99	0.99	2.15	0.15	0.46	0.41	1.07	0.52	1.14	1.42	1.00
S1	21.7	22.9	7.4	38.7	14.4	15.1	4.7	28.9	0.5	0.5	0.6	0.3	0.16	0.78	0.76	2.00	0.06	0.25	0.24	0.74	1.52	2.19	2.23	1.69
S2	33.0	33.3	4.7	47.4	25.4	25.6	3.2	37.3	0.3	0.3	0.5	0.3	0.16	1.15	1.14	2.02	0.15	0.53	0.51	1.07	0.03	1.18	1.25	0.88
S3	36.3	36.5	3.5	46.1	26.5	26.7	2.5	35.1	0.4	0.4	0.4	0.3	0.20	1.15	1.14	2.06	0.17	0.51	0.48	1.01	0.12	1.27	1.39	1.03
S4	38.5	38.8	4.9	61.5	29.0	29.2	3.5	42.7	0.3	0.3	0.4	0.4	0.39	0.98	0.90	2.15	0.21	0.46	0.41	0.87	0.91	1.14	1.20	1.47

Drill point angle of 118°

| | #15 C (Worse) F_z | | | | #10 C (Best) F_z | | | | | | | | #15 C (Worse) M_z | | | | #10 C (Best) M_z | | | | | | | |
	μ	rms	σ	P	μ	rms	σ	P	$\Delta\mu$	Δrms	$\Delta\sigma$	ΔP	μ	rms	σ	P	μ	rms	σ	P	$\Delta\mu$	Δrms	$\Delta\sigma$	ΔP
S	37.4	39.3	7.2	68.7	20.6	22.1	3.8	37.9	0.82	0.78	0.88	0.81	0.24	0.74	0.69	1.89	0.16	0.39	0.32	0.87	0.49	0.90	1.18	1.18
S1	38.7	40.1	10.6	68.7	12.0	13.1	5.2	29.5	2.22	2.06	1.03	1.33	0.12	0.48	0.47	1.22	0.09	0.20	0.17	0.56	0.34	1.46	1.70	1.18
S2	32.6	33.1	5.9	50.8	21.9	22.2	3.3	33.3	0.49	0.49	0.79	0.53	0.17	0.83	0.82	1.56	0.15	0.39	0.36	0.85	0.18	1.13	1.25	0.84
S3	36.2	36.7	6.1	51.4	25.3	25.6	3.8	37.9	0.43	0.43	0.61	0.36	0.28	0.70	0.84	1.87	0.20	0.44	0.39	0.87	0.39	0.59	1.13	1.16
S4	42.2	42.7	6.3	68.7	23.1	23.3	3.0	37.0	0.82	0.83	1.08	0.86	0.38	0.75	0.64	1.89	0.20	0.40	0.34	0.87	0.88	0.89	0.90	1.18

Drill point angle of 128°

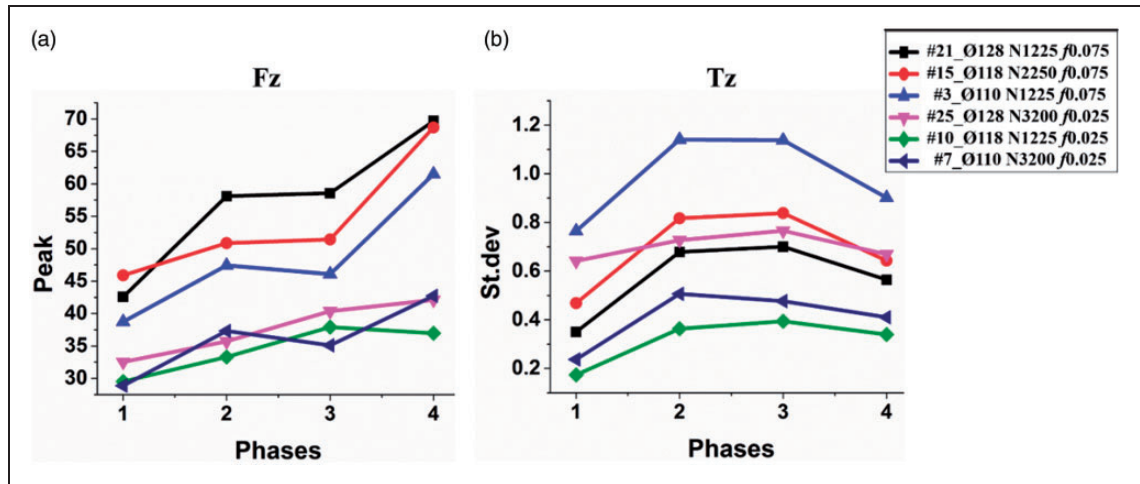| | #21 C (Worse) F_z | | | | #25 C (Best) F_z | | | | | | | | #21 C (Worse) M_z | | | | #25 C (Best) M_z | | | | | | | |
	μ	rms	σ	P	μ	rms	σ	P	$\Delta\mu$	Δrms	$\Delta\sigma$	ΔP	μ	rms	σ	P	μ	rms	σ	P	$\Delta\mu$	Δrms	$\Delta\sigma$	ΔP
S	34.6	39.3	7.4	69.7	21.4	24.5	5.4	42.1	0.62	0.61	0.38	0.65	0.15	0.65	0.57	1.80	0.17	0.69	0.70	1.65	−0.15	−0.06	−0.18	0.09
S1	20.9	23.7	11.1	42.6	12.7	14.7	7.4	32.5	0.65	0.61	0.49	0.31	0.09	0.36	0.35	0.93	0.19	0.67	0.64	1.65	−0.55	−0.46	−0.45	−0.44
S2	37.3	37.7	5.6	58.1	21.8	22.3	4.7	35.7	0.71	0.69	0.19	0.63	0.11	0.69	0.68	1.80	0.11	0.73	0.73	1.60	0.05	−0.06	−0.07	0.12
S3	38.5	39.0	6.0	58.6	25.9	26.3	4.9	40.4	0.49	0.48	0.24	0.45	0.20	0.73	0.70	1.47	0.19	0.79	0.77	1.46	0.06	−0.08	−0.09	0.00
S4	41.9	42.4	6.8	69.7	25.3	25.7	4.5	42.1	0.65	0.65	0.52	0.65	0.19	0.60	0.56	1.39	0.21	0.70	0.67	1.65	−0.07	−0.15	−0.16	−0.16

Figure 19. Variation of (a) peak thrust force and (b) standard deviation of torque for circularity.

Table 9. Different statistical parameter-based strategies for hole quality prediction.

Strategy no.	Model input function	Model output parameters
1	$f(\emptyset, N, f)$	F_d, R_z, C
2	$f(\emptyset, N, f, F_z \text{ (rms)})$	F_d, R_z, C
3	$f(\emptyset, N, f, F_z \text{ (peak)})$	F_d, R_z, C
4	$f(\emptyset, N, f, T_z \text{ (rms)})$	F_d, R_z, C
5	$f(\emptyset, N, f, T_z \text{ (peak)})$	F_d, R_z, C
6	$f(\emptyset, N, f, F_z \text{ (rms)}, F_z \text{ (peak)})$	F_d, R_z, C
7	$f(\emptyset, N, f, M_z \text{ (rms)}, T_z \text{ (peak)})$	F_d, R_z, C

specific hole characteristics like surface roughness and delamination, respectively, these were not found to be better than rms value in each hole quality feature extrapolation. The root means that the square value is also highly correlated with the mean as well as the standard deviation value, which indicates average along with the associated fluctuation of thrust force or torque in the present case. Therefore, global rms was considered with the local peak as an input to the hole quality feature models to improve the degree of fitness. Thus, various significant statistical feature-based strategies have been considered to improve the drilled hole quality predictability, as shown in Table 9. The three primary process variables, i.e. drill spindle revolutions per minute, feed rate, and point angle, were considered as inputs in strategy #1, whereas rms and peak value of thrust force and torque were included as significant sensory input individually with three process parameters in strategy #2 to #5 (Table 9). Finally, both rms and peak of thrust force as well as torque considered two more sensory inputs with three process variables in strategy #6 and #7 to compare the predictability between thrust force and torque in the drilling of CFRP laminates.

The model adequacy parameters such as *R*-square value, *F*-value, and *P*-value of the second-order regression models of each hole characteristics have been indicated in Table 10. The absolute prediction error, i.e. the ratio of deviation of experimental from predicted value to experimental data, has also been calculated for each strategy-based model. The objective was to compare the predictability of different statistical parameter-based plans. The *P*-value and *F*-value with corresponding degrees of freedom were found to be highly adequate. The *R*-square value, as well as mean absolute prediction error (MAPE), was improved using each selected sensor-based feature over offline based strategy (#1). The *R*-square value was found to be maximum with minimum MAPE in strategy #2 for delamination, considering one sensory input at a time. Thus, rms thrust force was the most significant indicator of surface delamination.

Similarly, the peak value of torque was more significant in the prediction of internal surface roughness and circularity error of the drilled hole. The MAPE was reduced significantly in delamination (37.93%), surface roughness (51.81%) as well as circularity error (38.93%) prediction considering the best sensor-based statistical feature as shown. Thus, the thrust force (using rms and peak value altogether) was a slightly better indicator than torque in the identification of delamination, whereas it was reversed in circularity prediction. However, the drilling torque was a significantly better indicator (than thrust force) of surface roughness with a 15.33% reduction in.

The scatter diagram of absolute percent error (APE) in surface delamination of all the experimental drilled hole considering only process variables (strategy #1) and the minimum MAPE-based strategies using one and two significant sensor-based features with process parameters, respectively (i.e. strategy #2 and #6) have been presented with associated maximum deviation (under and overprediction) in Figure 20. The central zero lines indicated the experimental value of delamination, which was considered as a reference line. The model under-predicted value indicated positive APE, whereas over-prediction

Table 10. Comparative performance report for MAPE different strategy-based models.

Strategy no.	F_d				R_z				C			
	R^2	*F*-value	*P*-value	MAPE	R^2	*F*-value	*P*-value	MAPE	R^2	*F*-value	*P*-value	MAPE
I	0.950	40.340	0.000	0.290	0.979	97.400	0.000	0.965	0.866	13.680	0.000	1.274
2	0.984	61.590	0.000	**0.180**	0.984	62.580	0.000	0.812	0.952	19.890	0.000	0.821
3	0.967	29.490	0.000	0.207	0.984	61.980	0.000	0.834	0.894	8.430	0.000	1.056
4	0.961	24.780	0.000	0.258	0.994	167.900	0.000	0.481	0.933	13.990	0.000	0.867
5	0.962	25.530	0.000	0.253	0.995	179.840	0.000	**0.464**	0.954	20.880	0.000	**0.778**
6	0.990	40.920	0.000	**0.134**	0.995	78.730	0.000	0.424	0.973	14.560	0.000	0.584
7	0.989	34.800	0.000	0.137	0.996	107.610	0.000	**0.359**	0.977	16.780	0.000	**0.569**

Note. Bold values shows the minimum of MAPE values of the single sensor strategy and double sensor strategy respectively.
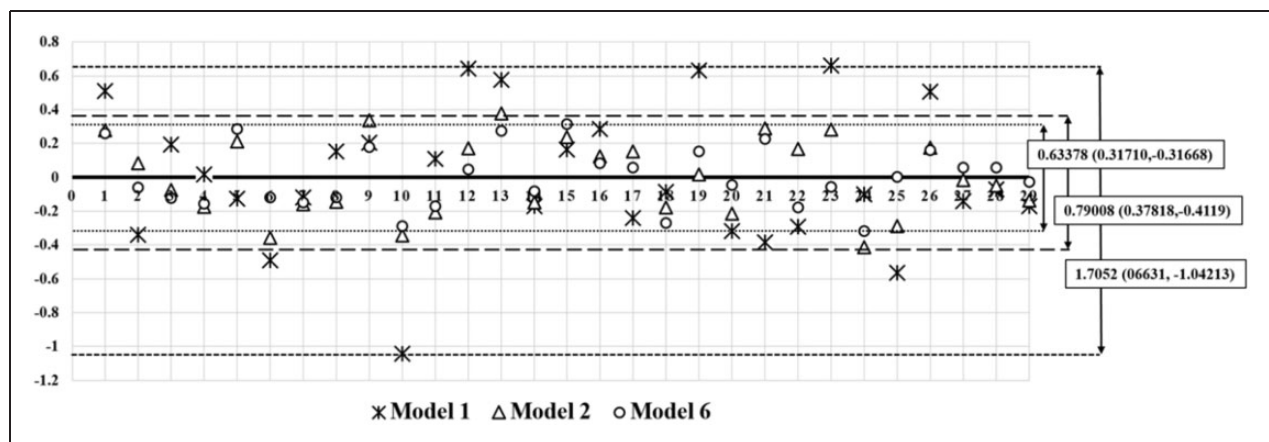
Figure 20. Comparative absolute error for delamination using a scatter diagram.
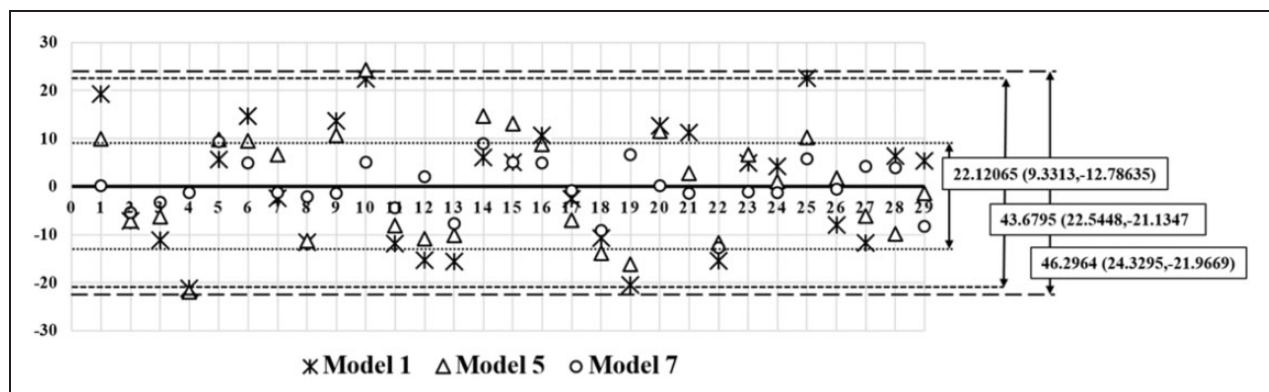
Figure 21. Comparative absolute error for surface roughness using a scatter diagram.

represented by negative APE as per reference zero error line as shown. The scatter plot for delamination error indicated symmetric data distribution concerning zero lines using each strategy. However, the deviation of APE without considering sensor-based features was found to be maximum (1.71%), which drastically reduced using one (0.79%) or two (0.63%) significant sensor-based features,

respectively, as shown. Thus, rms axial thrust force strongly correlated than peak thrust with surface hole delamination.

The scatter diagram of APE in surface roughness and circularity error has been indicated with associated maximum deviation (under and overprediction) in Figures 21 and 22, respectively. The drilling torque (strategy #5 and #7) was found to be the prime
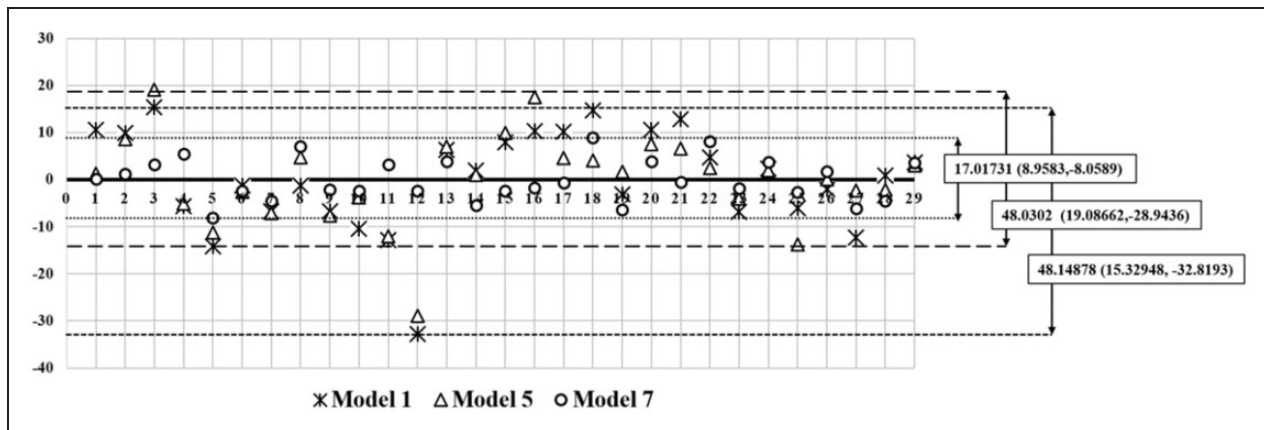
Figure 22. Comparative absolute error for circularity error using a scatter diagram.

indicator of these internal surface-related characteristics. The scatter plot for roughness, as well as circularity error, indicated symmetric data distribution using each strategy as found in case of delamination. The deviation of APE was almost found to be nearly the same considering fluctuation of torque (strategy #5) though MAPE significantly decreased. However, this APE deviation range was drastically reduced (more than 50%) considering both peak and rms value of torque altogether as shown. Thus, the root mean square value of torque (global) is highly essential along with peak value of torque (local) to predict drilled hole surface roughness of each experiment in a better way.

The same phenomenon has also been noticed in the prediction of the circularity error of the drilled hole. The scatter plot indicated more than 60% improvement in the APE deviation range using two significant sensor-based features (i.e. peak and rms value of torque) rather than only peak torque with process variables, as shown in Figure 22. Therefore, local peak torque (strategy #5) that did not wholly characterize the drilling process behavior through MAPE was found to be significant. However, the rms value of torque with peak torque (strategy #7) more accurately predicts the circularity error, as seen in the case of drilled hole surface roughness for CFRP composite laminates.

Concluding remarks

The machinability of bi-directional woven CFRP composite significantly influenced by surface delamination, roughness, and circularity error of the internal surface of the drilled hole. The axial thrust force with associated torque during drilling is highly essential to completely characterize the process. The response surface-based hole quality regression models as a function of process variables are highly feasible. The major research findings may be summarized as follows.

1. There are seven distinct phases starting from drill contact to departure through the laminate characterized by significant variation in thrust force and torque during drilling, out of which the first four phases can precisely indicate to drilled hole quality.
2. The axial thrust force with associated torque highly increases with an increase of feed rate, particularly using a higher drill point angle, whereas its fluctuation is compensated by an equivalent drop in torque variability to maintain the process stability.
3. The surface delamination with fiber pullout increases at a higher feed rate due to greater thrust force, which was found to be severe at low spindle speed with a high drill point angle. Thus, the internal surface roughness and the circularity error also improve at low feed rate with high spindle speed using a low drill point angle due to less torque fluctuation.
4. The minimum delamination was 1.075 at $\varnothing = 110°$, $N = 3200 \, \text{r/min}$, and $f = 0.025 \, \text{mm/rev}$ which was found to be the highest (1.147) at $\varnothing = 128°$, $N = 3200 \, \text{r/min}$, and $f = 0.075 \, \text{mm/rev}$. The surface roughness and circularity error were almost followed the similar parametric changes.
5. The axial thrust and torque fluctuation in the initial phases in the drilling cycle primarily indicate the delamination, whereas surface roughness and circularity error strongly correlated with a mean thrust with torque and peak thrust with torque instability, respectively, during last phases.
6. The surface delamination can be accurately predicted using axial thrust force than torque. The mean prediction error was significantly improved (37.9%) using rms thrust, which was further enhanced (53.8%) using both rms and peak thrust over off-line strategy. Thus, surface roughness and circularity error predictability improved (51.9–62.8%; 38.9–55.3%) using peak torque or both peak with rms torque.

7. The global rms value of thrust and torque is a better indicator of hole quality features than local peak value considering each drilling experiment separately.

Acknowledgements

Declaration of Conflicting Interests

The author(s) declared no potential conflicts of interest with respect to the research, authorship, and/or publication of this article.

Funding

ORCID iDs

Kamal Pal https://orcid.org/0000-0003-2122-6327
Karali Patra https://orcid.org/0000-0003-0133-2739

References

1. Soutis C. Carbon fibre reinforced plastics in aircraft construction. *Mater Sci Eng A* 2005; 412: 171–176.
2. Botelho EC, Silva RA, Pardini LC, et al. A review on the development and properties of continuous fiber/epoxy/aluminum hybrid composites for aircraft structures. *Mater Res* 2006; 9: 247–256.
3. Liu DF, Tang YJ and Cong WL. A review of mechanical drilling for composite laminates. *Compos Struct* 2012; 94: 1265–1279.
4. Karpat Y, Bahtiyar O, Değer B, et al. A mechanistic approach to investigate drilling of UD-CFRP laminates with PCD drills. *CIRP Ann – Manuf Technol* 2014; 63: 81–84.
5. López De Lacalle N, Lamikiz A, Campa FJ, et al. Design and test of a multitooth tool for CFRP milling. *J Compos Mater* 2009; 43: 3275–3290.
6. Singh I, Bhatnagar N and Viswanath P. Drilling of unidirectional glass fiber reinforced plastics: experimental and finite element study. *Mater Des* 2008; 29: 546–553.
7. Lee SC, Jeong ST, Park JN, et al. Study on drilling characteristics and mechanical properties of CFRP composites. *Acta Mech Solid Sin* 2008; 21: 364–368.
8. Jinyang XU and Ali Mkaddem MEM. Recent advances in drilling hybrid FRP–Ti composite – a state-of-the-art review. *Compos Struct* 2016; 135: 316–338.
9. Davim JP, Reis P and António CC. Drilling fiber reinforced plastics (FRPs) manufactured by hand lay-up: Influence of matrix (Viapal VHP 9731 and ATLAC 382-05). *J Mater Process Technol* 2004; 155–156: 1828–1833.
10. Gay D, Hoa SV and Tsai SW. *Composite materials: design and applications*. New York: CRC Press, 2002.
11. Xu J and El Mansori M. Experimental studies on the cutting characteristics of hybrid CFRP/Ti stacks. *Proc Manuf* 2016; 5: 270–281.
12. Chen W. Some experimental investigations in the drilling of CFRP composite laminates. *Int J Mach Tools Manuf* 1997; 37: 1097–1108.
13. Davim JP, Reis P and António CC. Experimental study of drilling glass fiber reinforced plastics (GFRP) manufactured by hand lay-up. *Compos Sci Technol* 2004; 64: 289–297.
14. Sinmazçelik T, Avcu E, Bora MÖ, et al. A review: fibre metal laminates, background, bonding types and applied test methods. *Mater Des* 2011; 32: 3671–3685.
15. Hufenbach W, Dobrzański LA, Gude M, et al. Optimisation of the rivet joints of the CFRP composite material and aluminium alloy. *J Achiev Mater Manuf Eng* 2007; 20: 119–122.
16. Barik T and Sarangi S. Assessment on hole quality during drilling of Al/CFRP stack. In: *Advances in unconventional machining and composites*. Singapore: Springer Singapore, 2020, pp.757–770.
17. Xu J, Li C, Mi S, et al. Study of drilling-induced defects for CFRP composites using new criteria. *Compos Struct* 2018; 201: 1076–1087.
18. Hocheng H and Tsao CC. The path towards delamination-free drilling of composite materials. *J Mater Process Technol* 2005; 167: 251–264.
19. Khashaba UA, El-Sonbaty IA, Selmy AI, et al. Machinability analysis in drilling woven GFR/epoxy composites: part I: effect of machining parameters. *Compos Part A Appl Sci Manuf* 2010; 41: 391–400.
20. Khashaba UA, Seif MA and Elhamid MA. Drilling analysis of chopped composites. *Compos Part A Appl Sci Manuf* 2007; 38: 61–70.
21. El-Sonbaty I, Khashaba UA and Machaly T. Factors affecting the machinability of GFR/epoxy composites. *Compos Struct* 2004; 63: 329–338.
22. Krishnamurthy RSK. Neural network thrust force controller to minimize delamination during drilling of graphite-epoxy laminates. *Int J Mach Tools Manuf* 1996; 36: 985–1003.
23. Xu J, Li C, Chen M, et al. An investigation of drilling high-strength CFRP composites using specialized drills. *Int J Adv Manuf Technol* 2019; 103: 3425–3442.
24. Barik T, Parimita S and Pal K. Parametric study and process monitoring on drilling of CFRP composites. In: *Proceedings of the 10th international conference on precision*, Meso, Micro Nano Engineering (COPEN 10), IIT Madras, 2017, pp.953–957.
25. Romoli L and Lutey AHA. Quality monitoring and control for drilling of CFRP laminates. *J Manuf Process* 2019; 40: 16–26.
26. Gaitonde VN, Karnik SR, Rubio JC, et al. Analysis of parametric influence on delamination in high-speed drilling of carbon fiber reinforced plastic composites. *J Mater Process Technol* 2008; 203: 431–438.
27. Khashaba UA. Delamination in drilling GFR-thermoset composites. *Compos Struct* 2004; 63: 313–327.
28. Xu J, An Q, Cai X, et al. Drilling machinability evaluation on new developed high-strength T800S/250F CFRP laminates. *Int J Precis Eng Manuf* 2013; 14: 1687–1696.
29. Fernández-Pérez J, Cantero JL, Díaz-Álvarez J, et al. Influence of cutting parameters on tool wear and hole

quality in composite aerospace components drilling. *Compos Struct* 2017; 178: 157–161.

30. Kilickap E. Optimization of cutting parameters on delamination based on Taguchi method during drilling of GFRP composite. *Expert Syst Appl* 2010; 37: 6116–6122.

31. Karnik SR, Gaitonde VN, Rubio JC, et al. Delamination analysis in high speed drilling of carbon fiber reinforced plastics (CFRP) using artificial neural network model. *Mater Des* 2008; 29: 1768–1776.

32. Hrechuk A, Bushlya V and Ståhl JE. Hole-quality evaluation in drilling fiber-reinforced composites. *Compos Struct* 2018; 204: 378–387.

33. Xu J, Li C, Dang J, et al. A study on drilling high-strength CFRP laminates: frictional heat and cutting temperature. *Materials (Basel)* 2018; 11: 2366.

34. Raj DS and Karunamoorthy L. Study of the effect of tool wear on hole quality in drilling CFRP to select a suitable drill for multi-criteria hole quality. *Mater Manuf Process* 2016; 31: 587–592.

35. Fernandes M and Cook C. Drilling of carbon composites using a one shot drill bit, part I: five stage representation of drilling and factors affecting maximum force and torque. *Int J Mach Tools Manuf* 2006; 46: 70–75.

36. Faraz A, Biermann D and Weinert K. Cutting edge rounding: an innovative tool wear criterion in drilling CFRP composite laminates. *Int J Mach Tools Manuf* 2009; 49: 1185–1196.

37. Maji K, Pratihar DK and Nath AK. Experimental investigations and statistical analysis of pulsed laser bending of AISI 304 stainless steel sheet. *Opt Laser Technol* 2013; 49: 18–27.

38. Romoli L and Lutey AHA. Quality monitoring and control for drilling of CFRP laminates. *J Manuf Process* 2019; 40: 16–26.

Appendix

Notation

C	circularity error
D	diameter of drill in mm
D_{max}	maximum diameter of delamination
D_{nom}	nominal diameter of the drilled hole
f	feed rate in mm/rev
F_d	delamination factor
F-value	a ratio of two variables
F_z	thrust force
F_z (peak)	peak value of thrust force
F_z (rms)	root mean square of thrust force
N	spindle speed in r/min
p	peak value
P-value	probability
R_a	roughness factor
R_z	avg. 10-point roughness factor
Tz	torque
Tz (peak)	peak value of torque
Tz (rms)	root mean square of torque
V_f	fiber volume fraction
w	web thickness in mm
α	clearance angle in °
β	helix angle in °
μ	mean
σ	standard deviation
Δ	difference
$\emptyset$	point angle in °